An Overview of Antarctic Sea Ice in the CESM2: Analysis of the Seasonal Cycle, Predictability, and Atmosphere-Ocean-Ice Interactions

Hansi K.A. Singh [1], Laura Landrum [2], and Marika M. Holland [2]

[1]School of Earth and Ocean Sciences, University of Victoria, Victoria BC Canada

[2]Climate and Global Dynamics Laboratory, National Center for Atmospheric Research, Boulder CO USA

Key Points:

- Antarctic sea ice is thinner and less extensive in the CESM2 than in the older CESM1.
- Different ice thermodynamics, and different coupled atmosphere and ocean states, account for different sea ice seasonal climatologies.
- Sea ice in the CESM2 is less predictable and less persistent than in the older CESM1.

Corresponding author: H.K.A. Singh, `hansingh@uvic.ca`

Abstract

We assess Antarctic sea ice climatology and variability in the CESM2, and compare it to that in the CESM1 and (where appropriate) real-world observations. In the CESM2, Antarctic sea ice is thinner and less extensive than in the CESM1, though sea ice area (SIA) is still approximately 1 million km^2 greater in the CESM2 than in observations. Though there is less Antarctic sea ice in the CESM2, the annual cycle of ice growth and melt is more vigorous in the CESM2 than in the CESM1. A new mushy-layer thermodynamics formulation implemented in the latest version of CICE in the CESM2 partially accounts for both greater frazil ice formation in coastal polyñyas and more snow-to-ice conversion near the edge of the ice pack in the new model. Basal melt, coastal ice divergence, and frazil growth are also more substantial in the CESM2 than the CESM1 due to a confluence of atmospheric and oceanic processes. In the CESM2, monthly SIA is less variable, annual mean SIA is less persistent, and monthly SIA is less predictable than in the CESM1. Upper ocean temperatures under the seasonal ice pack do confer some interannual predictability to Antarctic September SIA, though the relationship is weaker in the CESM2 than the CESM1. On the other hand, variability in upper ocean temperatures equatorward of the ice edge appear to follow, rather than lead, SIA variability in both models, suggesting that the state of the open Southern Ocean may be a poor predictor of ice evolution.

Plain Language Summary

Sea ice is a central part of the Antarctic climate system, and Earth system models are an indispensable tool for studying the climate of the Antarctic. Advances in modelling are essential for understanding and projecting future changes in the region as the globe warms. Here, we describe Antarctic sea ice climatology in the state-of-the-art Community Earth System Model, version 2 (CESM2). The CESM2 incorporates several modelling advances which collectively improve representation of Antarctic climate compared to previous model versions. Among these is a 'mushy layer' treatment of sea ice, where the ice is modelled as a mixture of solid ice and salty water. Modeling sea ice as a mushy layer changes the way that Antarctic sea ice grows in the CESM2, in a manner more closely resembling how Antarctic sea ice has been observed to grow in the real world. Antarctic sea ice area in the CESM2 also more closely matches observed sea ice area, due primarily to differences in atmospheric winds and ocean heating. In conjunction with ob-

servations and other state-of-the-art global climate models, the CESM2 will be an important tool for furthering understanding of Antarctic climate at present and in the future.

1 Introduction

Sea ice is a fundamental, dynamic component of the Antarctic climate system. Antarctic sea ice undergoes extraordinary expansion and retreat over the seasons: ice area expands from a mere 2 million km^2 at its end-of-summer minimum to nearly 15 million km^2 at its spring maximum, an expansion nearly twice the area of the Antarctic continent itself (Gordon, 1981; Parkinson & Cavalieri, 2012). This massive seasonal growth and retreat of ice area impacts nearly every aspect of the Antarctic system, from atmospheric stability and ocean dynamics, to ice sheet mass balance and biological productivity.

The presence of sea ice strongly attenuates (turbulent and radiative) heat and momentum conveyance between the atmosphere and ocean (Eicken, 2003), and the state of the lower troposphere in the high latitudes, including cloudiness, boundary layer depth, and stability, varies substantially with sea ice cover (see, e.g., Wall et al., 2017). Sea ice melt and growth impact ocean hydrography through freshwater capping and brine rejection, respectively (Pellichero et al., 2017); brine rejection plays a crucial role in creating high-density shelf waters off the Antarctic coast that form Antarctic Bottom Water, the coldest and densest water in the world oceans (Goosse et al., 1997; Ohshima et al., 2013). Dynamic calving from marine ice shelves, which flow from the Antarctic ice sheet, may be thwarted by the presence of sea ice cover or hastened by its absence (Massom et al., 2018). The Southern Ocean food web, essential for global food security, depends on the seasonal cycle of sea ice, with several keystone species relying on sea ice cover over the course of their developmental cycles (Garrison & Buck, 1989). The Antarctic climate system, both present and future, cannot be understood in full without a reasonable reckoning of the sea ice and its seasonality.

Antarctic sea ice differs in many respects from Arctic sea ice. The magnitude of the seasonal cycle over the Arctic is smaller than that over the Antarctic, with multi-year ice dominating much of Arctic icepack volume historically. Antarctic sea ice is thinner and more extensive (particularly in winter), while Arctic sea ice is thicker and more contained in area (Rothrock et al., 1999; Worby et al., 2008), as the Arctic basin is nearly

landlocked by the North American and Eurasian continents. As Antarctic sea ice extends further equatorward than Arctic sea ice, it is more exposed to fluctuations in the surface westerly wind maximum, and its variability is closely tied to the Southern Annular Mode (SAM; Kwok & Comiso, 2002; Simpkins et al., 2012; Raphael & Hobbs, 2014; M. Holland et al., 2017) and related Amundsen Sea Low (M. Holland et al., 2018). Mechanisms of ice growth and melt also differ between the two hemispheres. Much Antarctic sea ice growth occurs in polyñyas off the coast, as downslope (katabatic) winds flow from the high-elevation ice sheet to open coastal waters, driving frazil ice formation (Maqueda et al., 2004; Tamura et al., 2008). Snow falling over the ice pack also thickens Antarctic ice more so than Arctic ice, as snow weight lowers the freeboard below the sea surface, initiating snow-to-ice conversion (Eicken et al., 1995; Massom et al., 2001; Maksym & Markus, 2008). In spring and summer, Antarctic sea ice melts from its base as it retreats to its end-of-summer minimum, while Arctic ice melts at both top and bottom faces nearly equally (Perovich et al., 2014). Such differences between the hemispheres indicate that Antarctic sea ice must be understood as a component in a unique coupled system, distinct from that of the Arctic.

Antarctic sea ice has also responded very differently to a warming climate than Arctic sea ice. While Arctic sea ice has retreated significantly in response to anthropogenic greenhouse gas forcing, Antarctic sea ice underwent a modest expansion from 1979 to 2015. This paradoxical expansion of Antarctic sea ice area, occurring concurrently with increasing global mean surface temperatures and rapid retreat of Arctic sea ice, was initially attributed to stratospheric ozone loss over the Antarctic (J. Turner et al., 2009), or to an increase in freshwater fluxes into the Southern Ocean (due to ice shelf melt, for example; see Bintanja et al., 2013). Later studies suggested that neither the Antarctic ozone hole and associated positive SAM trend (Sigmond & Fyfe, 2010; Bitz & Polvani, 2012) nor observed changes in freshwater forcing (Swart & Fyfe, 2013; Pauling et al., 2016) were sufficient to explain Antarctic ice area expansion. Natural variability in sea ice area, either driven by variability in Southern Ocean temperatures (Singh et al., 2019), variability in Southern Ocean deep convection (Zhang et al., 2019), or variability in the tropics (Meehl et al., 2016), appears to be the simplest explanation for Antarctic sea ice area expansion over the satellite era. While Arctic sea ice area has experienced fluctuations due to natural variability over the satellite era (Swart et al., 2015), natural variability may play a greater role in Antarctic sea ice evolution because the response to greenhouse

gas forcing, both transient and equilibrium, is weaker in the Antarctic than the Arctic (Armour et al., 2016; Singh et al., 2018).

Changes in Antarctic sea ice impact not only the climate local to the Antarctic, but also climate elsewhere. Idealized atmospheric dynamical core experiments suggest that lower tropospheric heating in the high latitudes, similar to that resulting from sea ice loss, tends to push the eddy-driven jet and storm-track equatorward (McGraw & Barnes, 2016). Experiments which isolate the global climate response to (projected) late 21st century Arctic sea ice loss indicate a range of far-reaching impacts, including equatorward jet shifts in both hemispheres, a northward shift in the Intertropical Convergence Zone, and greater extratropical precipitation in both hemispheres (in a fully-coupled model; see Deser et al., 2015; Blackport & Kushner, 2017; Smith et al., 2017). Similar experiments performed to isolate the global climate response to Antarctic sea ice loss suggest a similar slew of remote responses, albeit weaker than the response to Arctic sea ice loss (England et al., 2018).

Though the local and global climate impacts of Antarctic sea ice are substantial, the study of Antarctic sea ice is hampered by the difficulty of obtaining *in situ* observations from remote regions with extreme climatic conditions. As such, global climate models employing sophisticated sea ice components, in which ice evolution is treated both thermodynamically and dynamically, are indispensable tools for study of the Antarctic climate system and its future fate.

Here, we present an overview of Antarctic sea ice seasonal climatology (including growth and melt processes), persistence, and predictability in a newly-developed, state-of-the-art global climate model, version 2 of the Community Earth System Model (CESM2; see Danabasoglu et al., 2019). The sea ice model in the CESM2 is CICE5 (Hunke et al., 2015; Bailey et al., 2020, submitted), which employs a mushy-layer thermodynamics scheme (Feltham et al., 2006; A. Turner & Hunke, 2015), supplanting the constant salinity scheme used in earlier versions of the model (Bitz & Lipscomb, 1999, hereafter BL99). Incorporating prognostic salinity has been shown to improve representation of sea ice growth, melt, the ice thickness distribution, and ocean-ice interactions in both hemispheres in models (Vancoppenolle et al., 2009; A. Turner & Hunke, 2015), making it a significant advance in sea ice modelling.

In our analysis, we compare and contrast Antarctic sea ice pre-industrial climatology in the CESM2 to that in the older CESM1, and, where possible, present-day observations. We first evaluate how differing Antarctic sea ice seasonal climatologies in the CESM2 and CESM1 are likely due, in some respects, to differences in their thermodynamics treatments, or, in other respects, to differences in their coupled atmosphere and ocean counterparts (section §3.1). We then evaluate differences in sea ice persistence and predictability between the CESM2 and the CESM1 (section §3.2). Finally, we consider thermodynamic coupling between the sea ice and ocean, and the extent to which ocean temperature anomalies may be useful for predicting Antarctic sea ice area in future months (section §3.3). We conclude by discussing several promising future research directions in the coupled evolution of Antarctic sea ice highlighted by our analysis (§4).

2 Methodology

The state-of-the-art version 2 of the Community Earth System Model (CESM2) is described in detail in Danabasoglu et al. (2019). All model components have been updated extensively, incorporating cutting-edge physics essential to accurate simulation of the Earth system. The atmosphere component of the CESM2, CAM6 (Bogenschutz et al., 2018), incorporates several parameterization advances, including a new unified atmospheric convection scheme (CLUBB; see Guo et al., 2015; Larson, 2017), updated cloud microphysics (Gettelman & Morrison, 2015; Gettelman et al., 2015), aerosol impacts on cloud formation (i.e. the aerosol indirect effect; see Hoose et al., 2010; Wang et al., 2014; Shi et al., 2015), and more sophisticated treatments of orographic drag (Scinocca & McFarlane, 2000; Beljaars et al., 2004). Other model components, including the land, ocean, and coupler, have also been updated (Danabasoglu et al., 2019).

The new CICE5 is described in depth by Hunke et al. (2015) and Bailey et al. (2020, submitted). The most significant advance in the new model is in the treatment of sea ice as a mushy layer, an amalgam of solid ice interspersed with microscopic pockets of brine (Feltham et al., 2006; A. Turner & Hunke, 2015). In this case, the enthalpy of the ice, q, is a weighted average of the enthalpy of the ice, q_i, and the enthalpy of the brine, q_{br}:

$$q = (1 - \phi)q_i + \phi q_{br} \ , \tag{1}$$

where ϕ is the fraction of the sea ice mush made up of liquid brine. The enthalpy of the ice evolves according to

$$\frac{\partial q}{\partial t} = \frac{\partial}{\partial z}\left(K\frac{\partial T}{\partial z}\right) + w\frac{\partial q_{br}}{\partial z} + F \ , \tag{2}$$

where T is the temperature of the mush, K is the vertical conductivity, w is the Darcy velocity of the brine (used for parameterizing rapid and slow modes of gravity-driven brine drainage; see A. Turner et al., 2013), and F represents the external energy flux to the ice (from atmosphere or ocean). The (bulk) salinity of the ice ($S = \phi S_{br}$) is a prognostic variable, and is computed as

$$\frac{\partial(\phi S_{br})}{\partial t} = w\frac{\partial S_{br}}{\partial z} + G \ , \tag{3}$$

where G is a source term. Inclusion of prognostic salinity into ice thermodynamics requires modifications in the calculation of the ice thermal conductivity, basal growth rate, frazil growth rate, rate of snow-to-ice conversion, and melt pond flushing (see A. Turner & Hunke, 2015). Compared to constant-salinity sea ice thermodynamics (see Bitz & Lipscomb, 1999), mushy layer thermodynamics augments both frazil and snow-to-ice growth: ice growth over open water occurs more readily with less heat loss to the atmosphere, as new ice is represented as an amalgam of solid ice and brine; and conversion of snow to ice is greater, as the thickness of the newly formed ice is reckoned to be that of the seawater-flooded snow, not compacted snow (A. Turner & Hunke, 2015).

Antarctic sea ice seasonal climatology and variability in the CESM2 are evaluated over the final 600 years of a 1100-year preindustrial run, where the atmospheric CO_2 concentration is fixed at 280 ppm and all other atmospheric constituents are held at preindustrial levels (see Danabasoglu et al., 2019). Sea ice seasonal climatology and variability in the CESM2 is compared to that over years 1100 to 1700 of the CESM1 Large Ensemble preindustrial run (Kay et al., 2015).

It is not necessarily appropriate (or useful) to compare the CESM2 and CESM1 pre-industrial control experiments directly with observations over the satellite era, as present-day sea ice conditions have been subject to a variety of modern-day forcings, including greenhouse gases and stratospheric ozone depletion over the South pole, which were not present in the pre-industrial climate. However, where reasonable, we compare Antarctic sea ice climatologies from the CESM2 and CESM1 preindustrial experiments with observations of Antarctic sea ice area from 1979 to 2018, collected through passive mi-

crowave satellite retrieval and processed through NASA Team and Bootstrap algorithms (Cavalieri et al., 1996, updated yearly, 1999; Comiso & Nishio, 2008).

3 Results

3.1 The Seasonal Cycle

We begin by comparing the seasonal cycle in monthly mean Antarctic sea ice area in the CESM2, CESM1, and satellite observations from 1979 to 2018 (Fig 1). Antarctic sea ice has a substantial seasonal cycle: sea ice cover expands to an area double that of the Antarctic continent every winter, but melts away nearly to the coast by the end of summer (Gordon, 1981). Overall, both models agree on the phasing of the sea ice seasonal cycle, and closely follow that of the satellite era observations. In both models and in observations, Antarctic sea ice area is minimal in February and maximal in September (Fig 1a). The sea ice growth season extends from March through August, while the melt season is from October through January; sea ice growth and melt, however, do occur year-round regionally in both the CESM2 and CESM1, as we describe further below.

The CESM2 has significantly less Antarctic sea ice area than the CESM1 year-round: September sea ice area is approximately 1.5 million km^2 lower in the CESM2 (15.9 million km^2 in the CESM2 compared to 17.4 million km^2 in the CESM1), while February sea ice area is approximately 1.0 million km^2 lower (2.7 million km^2 in the CESM2 versus 3.7 million km^2 in the CESM1). Though the CESM2 has considerably less sea ice area than the CESM1, sea ice area observed over the satellite era (1979 to 2018) is still approximately a half a million to a million km^2 less than that in the CESM2 in the annual mean (Fig 1a, compare solid and dashed blue lines and with solid black line; Antarctic sea ice area in the NASA Team-processed satellite observations are approximately 0.4 million km^2 less than that in the CESM2 in the annual mean, while ice area in the Bootstrap-processed observations are approximately 1.0 million km^2 less than that in the CESM2 in the annual mean). Greater sea ice area in the CESM2 relative to satellite era observations may either reflect systematic biases in the CESM2, or reflect the very different forcings present over the late 20th and early 21st centuries, compared to those imposed in the CESM2 pre-industrial experiment. Indeed, historical CESM2 runs

evince much closer agreement between modelled sea ice area and observations (DuVivier et al., 2019, submitted).

We compare interannual variability in the sea ice seasonal cycle between the CESM2, CESM1, and satellite-era observations by comparing their standard deviations in monthly sea ice area (Fig 1b). In general, the CESM2 has less variability in monthly sea ice area than the CESM1, particularly from April to November, encompassing the mid- to late-growth season and early melt season (Fig 1b, compare solid and dotted black lines). We further assess the variability in monthly mean sea ice area in the two models by computing the monthly sea ice area standard deviation in the models using all contiguous 40-year segments sampled from each pre-industrial control experiment, and comparing the envelope of these standard deviations (Fig 1b, yellow and grey shaded regions show the standard deviation range in the CESM2 and CESM1, respectively) to the monthly standard deviations in sea ice area from the last 39 years of the observations (Fig 1b, solid blue line). Over much of the seasonal cycle, the monthly sea ice area standard deviation in the observations falls within (or nearly within) the range of that in both models. However, the variability in the observations substantially exceeds that in both models in the middle of the melt season (November and December; compare shaded yellow and grey regions to blue line in Fig 1b), suggesting that both models may have too little interannual variability in the hemispheric total sea ice area at this time of year.

In Figure 2, we compare sea ice area and extent between the CESM2 and CESM1, focusing on the annual mean, summer (December, January, and February average; DJF), and winter (June, July, and August average; JJA). Reduced sea ice area and extent in the CESM2, relative to the CESM1, is evident over most sectors and seasons around the continent, particularly the Ross Sea, Weddell Sea, and south Indian Ocean; only the Amundsen-Bellinghausen sector shows slightly greater sea ice extent in the CESM2 compared to the CESM1, especially in winter (JJA; compare Figs 2e, f). In summer (DJF), decreased sea ice area and extent in the CESM2 is evident around the whole continent, as the sea ice edge retreats substantially further towards the Antarctic coast in the CESM2 compared to the CESM1 (Figs 2c, d).

Differences between the CESM2 and CESM1 are also evident in the interannual variability of the location of the ice edge (Fig 2, dashed red lines). In both the CESM2 and CESM1, interannual variability in the ice edge is greatest over the West Antarctic

sectors, particularly the Weddell and Amundsen-Bellinghausen Seas in summer (Figs 2c, d) and winter (Figs 2e, f). In summer, substantial interannual variability in the sea ice edge is also present over the South Indian sector of the East Antarctic in the CESM1, but not the CESM2.

In addition to having reduced area and extent, Antarctic sea ice is also thinner in the CESM2 than the CESM1 (Fig 3, colors). Because sea ice is thinner and less extensive in the CESM2, there is less ice volume in the CESM2 (13.8×10^3 km^3 in the CESM2 compared to 14.6×10^3 km^3 in the CESM1). There is also notable regional heterogeneity in sea ice thickness, which also differs between the two models. In both models, sea ice is thinnest over the East Antarctic sectors, and thickest over the West Antarctic: ice is thickest in the Amundsen, Bellinghausen, and Ross seas in the CESM1 (Fig 3a), and in the Amundsen and western Weddell seas in the CESM2 (Fig 3b). In the CESM1, sea ice remains thick over the Amundsen-Bellinghausen sector in summer (Fig 3c), and also thickens over the Ross and Weddell sectors in winter (Fig 3e). In the CESM2, on the other hand, ice remains thick over the Amundsen and eastern Weddell Seas in summer (Fig 3d), and also thickens over the Bellinghausen, western Weddell, and Ross Seas in winter (Fig 3f). Thick ice also hugs much of the Antarctic coast in the CESM2, even in summer (Fig 3d). These regions of thicker coastal sea ice (reminiscent of land-fast sea ice) are particularly evident over the East Antarctic in the CESM2, but are notably absent in the CESM1 (compare Fig 3b and a).

Thinner sea ice in the CESM2 also corresponds to warmer surface temperatures over the ice pack (compare the 260K isotherm in Figs 3a and b). In summer, a substantial portion of the ice pack in the CESM2 reaches the melting temperature: the 270K isotherm follows the Antarctic coast over nearly all sectors (except the Weddell; see Fig 3d). In the CESM1, on the other hand, the 270K isotherm is distant from the coast, particularly over West Antarctic sectors (Fig 3c), indicating that much of the ice pack over this region never reaches the melting temperature at the surface. In winter, surface temperatures are also greater in the CESM2 than the CESM1 (compare Figs 3f and e), as thinner sea ice has a greater equilibrium radiative temperature at its top surface than thicker ice, all other factors being equal (see Thorndike, 1992; Leppäranta, 1993).

The seasonal cycle of hemispheric total ice growth and melt also differs substantially between the CESM2 and the CESM1. In general, the rates of ice growth and melt

are larger in the CESM2 than the CESM1 (Fig 4, compare solid and dotted lines), suggesting that the sea ice annual cycle is more intense in the CESM2 than the CESM1. In both models, ice grows most rapidly during the growth season (March through August) and melts most rapidly during the melt season (October through January); however, ice growth also occurs during the melt season, and ice melt also occurs during the growth season, albeit at lower rates. The rate of sea ice growth in the CESM2 exceeds the rate of sea ice growth in the CESM1 year-round by up to 50%, with the largest differences between the two models occurring in the late growth season and early melt season (August to November; see Fig 4a). The rate of sea ice melt is also greater in the CESM2 over the growth season and the early melt season (April through November); however, the rate of ice melt in the CESM1 exceeds that in the CESM2 in the late melt season (January and February; Fig 4b), possibly because there is substantially more sea ice available to melt in the CESM1 than in the CESM2 at this point in time.

As described earlier in §2, the most significant difference between the sea ice formulations in the CICE5 (in the CESM2) versus the CICE4 (in the CESM1) is the mushy-layer thermodynamics in the former, which has supplanted the BL99 thermodynamics in the latter. However, neither the thinner ice pack nor the less extensive sea ice area in the CESM2, compared to the CESM1, is directly attributable to differences in the sea ice formulation; comparative studies of both thermodynamic formulations employed in the same sea ice model, with all other model components being identical, suggest that the mushy-layer formulation tends to thicken sea ice and increase the extent of the ice pack (A. Turner & Hunke, 2015; Bailey et al., 2020, submitted), which is opposite the differences we find between the CESM2 and CESM1. In the following sections, we further explore how differences in sea ice growth and melt, partly attributable to these different formulations of sea ice thermodynamics, interact with different atmospheric and oceanic factors in these two models to produce the distinct Antarctic sea ice climatologies reported here.

3.1.1 Sea Ice Growth

We now consider differences between sea ice growth in the CESM2 versus CESM1 in greater detail. The CICE model simulates three types of sea ice growth (Hunke & Lipscomb, 2008): frazil (open-water) growth, where sea ice forms over open water as ocean mixed layer temperatures drop below the freezing point; basal (congelation) growth, where

sea ice growth at the bottom surface of the ice is driven by conductive fluxes through the ice; and snow-to-ice growth, where snow is converted to ice when the weight of overlying snow depresses the top surface of the ice below the sea surface. Total sea ice growth, dh/dt_{growth}, is due to the sum of basal, frazil, and snow-to-ice growth components:

$$\left(\frac{dh}{dt}\right)_{growth} = \left(\frac{dh}{dt}\right)_{basal} + \left(\frac{dh}{dt}\right)_{frazil} + \left(\frac{dh}{dt}\right)_{snow} . \tag{4}$$

Figure 5 shows the relative contributions of frazil, basal, and snow-to-ice terms in monthly mean sea ice growth in the CESM2 and the CESM1. While basal growth is weaker in the CESM2 than the CESM1, frazil and snow-to-ice growth are more vigorous. Greater snow-to-ice and frazil growth, and decreased basal growth, are also found when mushy-layer thermodynamics replaces BL99 in the CICE5 within the fully-coupled CESM2 (Bailey et al., 2020, submitted), suggesting that differences between the CESM2 and CESM1 in the relative contributions of these sea ice growth terms can be attributed at least in part to their different thermodynamic formulations (mushy-layer in the CESM2/CICE5 versus BL99 in the CESM1/CICE4).

We now examine each of these sea ice growth terms in further detail. The frazil (open-water) sea ice growth rate is approximately twice as large in the CESM2 as in the CESM1 (Fig 5, compare solid and dotted teal lines), and the peak in frazil ice formation occurs slightly later in the growth season in the CESM2 (April in the CESM1 versus May in the CESM2). Greater frazil growth is facilitated by mushy-layer thermodynamics, as a brine-ice slurry can be formed with less latent heat exchange, compared to that required when ice salinity is assumed constant (A. Turner & Hunke, 2015). The spatial distribution of frazil sea ice growth also differs between the CESM2 and the CESM1 (compare Figs 6a, d, g with Figs 7a, d, g). While frazil growth can occur within the ice pack itself, particularly early in the season when the sea ice fraction is lower (see Figs 6a, 7a), most frazil growth occurs near the Antarctic coast in both models. However, coastal frazil growth is at least two to four times more vigorous in the CESM2 than the CESM1 throughout the growth season, especially over West Antarctic sectors.

Greater coastal frazil growth in the CESM2 is especially significant in light of *in situ* observations of Antarctic sea ice formation in winter, which document vigorous ice growth occurring within coastal polyñyas (Tamura et al., 2008). Such coastal latent heat polyñyas are driven by katabatic (down-slope) winds off the Antarctic continent, which elicit large turbulent fluxes from the ocean mixed layer, and advect newly-formed sea

ice away from the coast to expose more open water for further open-water sea ice growth (reviewed by Maqueda et al., 2004). Furthermore, buoyancy loss in these coastal polyñyas, through both surface heat loss and brine rejection from newly-formed sea ice, supports formation of Antarctic Bottom Water (AABW), the most dense water in the world ocean (Goosse et al., 1997; Ohshima et al., 2013). More vigorous frazil ice formation in coastal polyñyas in the CESM2 relative to the CESM1 hints at differences in AABW formation between the two models, and further exploration of such differences is warranted (but beyond the scope of the present study).

In both models, basal (congelation) growth is the largest contributor to sea ice thickening over much of the growth season. The basal growth rate is approximately 25% smaller in the CESM2 than the CESM1 throughout the growth season (Fig 5, compare solid and dotted turquoise lines), and the peak in basal growth is approximately one month later in the CESM1 than the CESM2 (June in the CESM1 versus May in the CESM2). The spatial distribution of basal growth is similar in both models: greatest near the Antarctic coast, particularly over the East Antarctic sectors, and smallest near the ice edge (Figs 6b, e, h and Figs 7b, e, h). Basal growth is comparable in magnitude between both models at the beginning of the growth season (compare Fig 6b with Fig 7b), but declines much more in the mid- and late- growth season in the CESM2 than the CESM1 (compare Figs 6e, h with Figs 7e, h). As we show later in §3.1.3, decreased basal growth in the CESM2 is likely due to greater ocean heat convergence under the ice pack in this model, compared to the CESM1.

As basal growth declines in the mid- to late- growth season in both models, snow-to-ice growth increases, peaking at the ice area maximum in September, and persisting through the early melt season (Fig 5, purple lines). Observations of sea ice growth in the Antarctic suggest that snow-to-ice growth is particularly important in this hemisphere (Jeffries et al., 2001; Maksym & Markus, 2008): the Antarctic ice pack is thinner than that of the Arctic, and snowfall is more plentiful because of the adjacent storm track, making snow-to-ice growth an important component of the sea ice budget (Eicken, 2003). Antarctic snow-to-ice growth is nearly twice as large in the CESM2 relative to the CESM1, and the greater ice growth rate in the CESM2 in the mid- to late- growth season and early melt season is entirely attributable to this term (recall Fig 4a). Unlike basal and frazil growth, which occur at the coast and at the center of the ice pack, snow-to-ice growth

occurs near the edge of the ice pack in both models (compare Figs 6c, f, i to Figs 7c, f, i).

Significantly greater snow-to-ice growth in the CESM2 is due, in part, to mushy-layer thermodynamics: because the mushy-layer formulation allows prognostic salinity within the ice, seawater flooding of snow layers is permitted as the weight of snow depresses ice below the water line, and the resulting ice growth is assessed to be the full depth of the flooded snow (i.e. snow plus brine; see A. Turner & Hunke, 2015). In the BL99 formulation, on the other hand, snow-to-ice growth is weaker because it is assumed that snow must be compressed to produce ice, thereby decreasing the thickness of ice that can be formed from the same quantity of snow. Thinner ice in the CESM2 also permits greater snow-to-ice growth, as less snow is required to depress the surface of the ice below the water line (recall Fig 3).

Furthermore, as shown in Figure 8, greater snow-to-ice growth in the CESM2 also occurs because of greater snowfall year-round over the ice pack. While there is greater snowfall equatorward of the ice edge in winter and spring in the CESM1 (Fig 8, brown colors north of the ice edge), there is greater snowfall poleward of the ice edge year-round in the CESM2 (green colors south of the ice edge). The latter increase permits more snow accumulation near the edge of the ice pack in the CESM2, and this snow is more readily converted to ice. Indeed, there is less snow depth over sea ice in the CESM2 than the CESM1 (not shown) though snowfall is greater, indicating more ready snow-to-ice formation in the former than in the latter.

We now consider relationships between frazil, basal, and snow-to-ice growth terms, as evaluated from lead-lag correlations between the area-integrated monthly mean value of each term with every other term (as shown in Fig 9). We find many similarities, but also significant differences, between these relationships in the CESM2 compared to the CESM1, suggesting that mechanisms driving interannual variability in sea ice growth (and, therefore, ice area, extent, and volume) likely differ between the two models.

We begin with the relationship between basal and frazil growth, which differs markedly between the two models (compare Figs 9a and b). In the CESM1, greater frazil growth over the growth season (February through September) is strongly correlated with greater basal growth over concurrent and subsequent months (Fig 9a, red region). Conditions that favor frazil growth (such as strong upward turbulent and net radiative fluxes from

surface to atmosphere) also favor basal growth, so the close correspondence between these two growth terms at zero lead-lag (i.e. concurrently) is unsurprising. Furthermore, frazil growth earlier in the season may be necessary for subsequent basal growth later in the season, as frazil growth provides a 'platform' of thin ice on which basal growth can commence. While these reasonable relationships between frazil and basal growth are clearly evident in the CESM1, they are nearly absent in the CESM2 (compare Figs 9a and b). This may be due to weak basal growth in the CESM2, relative to the CESM1, which disrupts these expected correlations between frazil and basal growth terms. Further study of these growth relationships in both models is warranted.

The relationships between basal and snow-to-ice growth are more qualitatively similar between the two models, though some differences are evident (compare Figs 9c and d). In both the CESM2 and CESM1, vigorous basal growth early in the growth season leads vigorous snow-to-ice growth later in the season (red regions in Figs 9c and d), likely because basal growth creates a base of ice on which snow can accumulate, facilitating snow-to-ice conversion. This relationship persists to the end of the growth season and the early melt season (through November) in the CESM1, but tapers away in the late growth season (through August) in the CESM2. While basal growth promotes subsequent snow-to-ice growth in both models, vigorous snow-to-ice growth in the mid- and late- growth season tends to inhibit concurrent and subsequent basal growth in both models (Figs 9c and d, blue regions). Snow-to-ice growth depends on snow cover, which insulates the top surface of the sea ice, thereby stymieing basal growth by decreasing the conductive flux through the ice (Powell et al., 2005). Furthermore, snow-to-ice growth will thicken the ice, which will also reduce the conductive flux through the ice and slow basal growth (Maykut & Untersteiner, 1971; Thorndike, 1992). Though the negative correlation between late-season snow-to-ice conversion and subsequent basal growth is present in both models, the relationship tapers away more rapidly in the CESM2 than the CESM1 (by September in the CESM2, but persisting through December in the CESM1).

The relationships between frazil growth and snow-to-ice growth are also qualitatively similar between the two models (Figs 9e, f). In both, greater frazil ice formation early in the growth season (February to April) tends to lead greater snow-to-ice growth later in the season (red regions in Figs 9e, f), though the relationship wanes more rapidly with lead time in the CESM2 than the CESM1. Later in the growth season, however, greater frazil ice formation is linked to less concurrent snow-to-ice growth (blue regions

near the dashed grey line in Figs 9e, f). Significant frazil growth later in the growth season may be an indicator of a sluggish growth season, implying a more limited base on which snow-to-ice conversion can occur. This latter relationship is conjectural, and more exploration of this point may be warranted.

3.1.2 Sea Ice Melt

While sea ice growth differs substantively between the CESM2 and the CESM1, sea ice melt is more qualitatively similar (Fig 10). The CICE model simulates three types of sea ice melt: basal (occurring at the bottom of the ice), lateral (occurring on the lateral edge of the ice), and top (occurring at the top face of the ice). Melt is greatest during the melt season, but substantial melt also occurs during the growth season (recall Fig 4). In both models, more than 95% of melt year-round occurs through basal melt (Fig 10, orange lines), with much smaller contributions from lateral and top melt during the mid- to late- melt season (November through February; red and goldenrod lines in Fig 10). This distribution of terms differs substantially from the melt budget in the Arctic, where top melt plays a much larger role (Andreas & Ackley, 1982).

In the CESM2, basal melt is greater than that in the CESM1 over much of the year, including over the growth season and the early melt season (March through November). Greater basal melt in the CESM2 is consistent with mushy-layer thermodynamics in this model, as the melt pond flushing and gravity drainage formulations promote more vigorous basal melt (A. Turner & Hunke, 2015; Bailey et al., 2020, submitted). However, basal melt in the CESM1 exceeds that in the CESM2 in the mid- to late- melt season (January and February), which may occur because there is significantly more ice remaining to melt in the CESM1 than the CESM2 at this point in time.

3.1.3 Dynamics and Thermodynamics

We now consider the interplay between the thermodynamics of ice growth and melt, described in the previous sections, and the dynamics of the coupled atmosphere and ocean. We begin by assessing the spatial pattern of changes in sea ice volume with time (i.e. the ice volume tendency), which is due to the sum of thermodynamic and dynamic terms:

$$\frac{dV}{dt} = \left(\frac{dV}{dt}\right)_{thermodynamics} + \left(\frac{dV}{dt}\right)_{dynamics}, \tag{5}$$

where the thermodynamic contribution to ice volume change, $dV/dt_{thermodynamics}$, is due to the growth (frazil, basal, and snow-to-ice) and melt (basal, lateral, and top) processes described previously; and the dynamic contribution, $dV/dt_{dynamics} = -\nabla \cdot (\vec{v}\, V)$, is due to advection by the local ice pack velocity $\vec{v}$ (Hunke & Lipscomb, 2008).

In Figure 11, we show the thermodynamic and dynamic contributions to the ice volume tendency in the CESM2 and the CESM1 over selected months spanning the seasonal cycle (December, February, June, and September). Overall, both models generally agree qualitatively regarding these thermodynamic and dynamic contributions to ice volume change, though important differences do exist, as we describe further below. Over the melt season (December and February; Figs 11a-d and 11e-h), there is a thermodynamic decrease in sea ice volume near the center and edge of the ice pack in both models (red regions in Fig 11a, b, e, f), driven primarily through basal melt (recall Fig 10). At the same time, there is a modest dynamic divergence of ice volume away from the coast (red regions in Figs 11c, d), and a modest dynamic convergence of ice volume near the ice edge (light blue regions near the black ice edge contour in Figs 11c, d). Dynamic divergence of ice away from the center of the ice pack during the melt season is slightly greater in the CESM2 than the CESM1 (compare Figs 11c and d), which may be a factor in promoting greater ice melt in this model, as ice melt occurs more readily near the edge of the ice pack than at the center.

Over the growth season (June and September; Figs 11i-l and 11m-p), ice volume increases through thermodynamic processes in both models (i.e. frazil, basal, and snow-to-ice growth, as described in §3.1.1; blue regions in Figs 11i, j, m, n), but also declines through melt at the ice edge (red regions near the black ice edge contour). At the same time, there is significant dynamic divergence of ice volume away from the coast and center of the ice pack in both the CESM2 and the CESM1 (red regions in Figs 11k, l, o, p), and dynamic convergence of ice towards the edge of the ice pack (blue regions near the black ice edge contour). Thus, over the course of the growth season, ice grows near the coast and the center of the ice pack, diverges away from these regions of growth, converges towards the edge of the ice pack, and melts at the ice edge.

Figure 12 highlights differences between the CESM2 and CESM1 in the relative contributions of thermodynamic and dynamic processes to the ice volume tendency over selected months spanning the growth season (April, June, and August; shown as the dif-

ference between the CESM2 and the CESM1). First, we examine differences in the thermodynamic contributions to the ice volume tendency between the CESM2 and CESM1 (Figs 12a, c, e). Over the course of the growth season, melt at the ice edge is significantly greater in the CESM2 than the CESM1 (red regions near the black ice edge contours). Greater melt at the ice edge in the CESM2 is evident nearly everywhere, including the Weddell and Ross sectors of the West Antarctic, and much of the East Antarctic. The Amundsen-Bellinghausen sector is one of the only regions where melt at the ice edge is not significantly greater in the CESM2 than the CESM1, though greater melt even here is evident near the end of the growth season (August; Fig 12e).

There are also differences in the dynamic contribution to ice volume change between the CESM2 and CESM1 (Figs 12b, d, f). First, there is greater dynamic divergence of sea ice away from the coast and the center of the ice pack in the CESM2 throughout the growth season (red regions in Figs 12b, d, f). Greater ice divergence is evident around much of the continent, and is particularly pronounced over the East Antarctic sectors, the Weddell Sea, and the Amundsen-Bellinghausen Seas. Greater transport of sea ice away from the Antarctic coast in the CESM2 may contribute to more vigorous frazil ice growth in coastal polyñyas in this model (recall Figs 5, 6, and 7). At the same time that more ice diverges away from the Antarctic coast in the CESM2, there is correspondingly greater dynamic convergence of sea ice towards the ice edge (blue regions near the black ice edge contours). Dynamic ice volume convergence near the ice edge in the CESM2 is pronounced around nearly the entire continent over the course of the growth season, though it is weakest circa the Ross sector.

To better understand the mechanisms responsible for these differences in the growth season ice volume tendency between the CESM2 and the CESM1, we first examine the sea level pressure in both models in Figure 13 (colors; shown for selected months spanning the growth season: April, June, and August). Both the CESM2 and CESM1 exhibit a distinct tripole of low sea level pressure centers circling the Antarctic continent (as has been analyzed previously by Raphael, 2004, 2007): over the Amundsen-Bellinghausen sector, the south Indian sector, and the western south Pacific sector. These low pressure centers are significantly deeper in the CESM2 than the CESM1 (compare Figs 13b, d, f with 13a, c, e), indicating greater stationary wave activity in the former than the latter (Raphael, 2004). As a result, there is greater advection of sea ice by the cyclonic quasi-geostrophic near-surface flows that arise from these low pressure centers in the CESM2

compared to the CESM1 (compare arrows in Figs 13b, d, f with 13a, c, e; also see Raphael, 2007). Consequently, more sea ice is transported away from the center of the ice pack and towards its edges in the CESM2, as suggested earlier by differences in the dynamic ice volume tendency in the two models (recall Fig 12).

Much stronger near-surface zonal winds accompany the stronger stationary wave activity in the CESM2, as shown in Figure 14. Both surface easterlies and westerlies are stronger year-round in the CESM2 relative to the CESM1 (colors in Fig 14; near-surface zonal winds in the CESM2 and the CESM1 are shown by the blue solid and blue dotted contours, respectively), indicating greater surface wind stress in the CESM2 than the CESM1. Despite substantially stronger zonal winds in the CESM2, the latitude of zero wind velocity (i.e. where easterlies transition to westerlies) is only slightly more equatorward in the CESM2 than the CESM1 (compare zero solid and dotted contours in Fig 14). As the meridional gradient in the zonal wind is greater in the CESM2 than the CESM1, there is greater wind stress curl over the ice pack and the Southern Ocean in the former than the latter.

Greater wind stress curl in the CESM2 also implies greater wind-driven upwelling beneath the ice pack in this model, relative to the CESM1. As waters at greater depth at this latitude are warmer than near-surface waters, greater upwelling results in greater heating by increased vertical advection (Fig 15, colors show the difference in heating by vertical motions between the CESM2 and the CESM1 in K/day). Greater heating by vertical upwelling in the CESM2 is most evident directly below the mixed layer under the seasonal ice pack (i.e., between the minima and maxima of ice extent, delineated by the vertical turquoise lines, and below the green lines denoting the base of the mixed layer), and tends to decrease the stratification of the water column; as a consequence, the thickness depth between the 27.3 and 27.7 isopycnal contours is approximately 50m greater under the ice pack in the CESM2 than the CESM1 (compare solid purple and dotted purple lines in Fig 15). Greater heating by vertical advection is also evident in the mixed layer itself, circa 60S, which corresponds to the location of the mean ice edge near the middle and end of the ice growth season.

Stronger surface wind stress, greater wind stress curl, more heating by vertical advection, and weaker ocean stratification all contribute to greater ocean heat flux convergence in the CESM2, relative to the CESM1, as shown in Figure 16. The monthly ocean

heat flux convergence in the mixed layer, Q, is calculated for both models as a residual from the month-to-month temperature tendency of the mixed layer, dT/dt, and the total surface heat flux, F_{sfc}:

$$\rho_W c_p H_{ML} \frac{dT}{dt} = Q + F_{sfc} \ , \tag{6}$$

where ρ_W is the density of seawater, c_p is its heat capacity, and H_{ML} is the mixed layer depth (see Bitz et al., 2012).

Compared to the CESM1, we find that the ocean heat flux convergence over the growth season is modestly greater under the ice pack and significantly greater at the ice edge in the CESM2. Early in the growth season, there is significantly greater ocean heat flux convergence under the ice pack in the CESM2 (April; Fig 16a), which persists to some extent over the course of the growth season (June through August; Figs 16b, c), and may limit basal growth (recall Fig 5) and sea ice thickness (recall Fig 3) in this model. In the mid- to late- growth season, greater ocean flux convergence is most evident at the ice edge in the CESM2 (June and August; Figs 16b, c), and is responsible for greater melt here (recall the more negative thermodynamic ice volume tendency at the ice edge in the CESM2 during the growth season, as shown in Figs 12a, c, e). Significantly, greater ocean heat flux convergence at the ice edge in the CESM2 coincides with areas where the ice edge is more poleward in the CESM2 relative to the CESM1; this is particularly evident in the eastern Weddell, Indian, and the Ross sectors, and suggests that greater ocean heating may play an important role in limiting sea ice extent in these regions in the CESM2. As greater wind stress and more intense stationary wave activity in the CESM2 diverges ice away from the Antarctic coast and center of the ice pack, greater ocean heat flux convergence simultaneously limits ice thickness and extent.

3.2 Persistence and Predictability

So far, we have focused on the seasonal cycle in Antarctic sea ice in the pre-industrial CESM2 experiment, and highlighted differences relative to the CESM1. We found that many of the differences in the seasonal cycle between the two models can be attributed to differences in sea ice thermodynamics (the mushy-layer formulation in the new CICE5 versus the BL99 formulation in the older CICE4), but differences in atmosphere and ocean dynamics are also crucial in explaining differences in ice area, volume, and extent.

Now, we consider interannual variability in sea ice area, and how this variability differs between the CESM2 and CESM1. We begin with the annual mean ice area over 600 years in the CESM2 and the CESM1, shown in Figure 17 (thin grey lines). Both models exhibit variability over a range of time scales, though no time scales emerge as statistically significant at the 95% confidence level for an AR1 red noise process (not shown). The two-standard deviation range of the annual mean ice area is approximately 0.2×10^6 km^2 greater in the CESM1 than the CESM2 (horizontal grey lines in Fig 17; 1.4×10^6 km^2 in the CESM2 versus 1.6×10^6 km^2 in the CESM1, which are statistically distinct at $p < 0.01$ using the UNOVA F-test).

Decreased variability in the CESM2 is also evident when we consider multi-decadal time periods when ice area trends are positive (i.e. when sea ice area is expanding over several decades). For each model, five 35-year time periods with the greatest positive ice area trends over 600 years are highlighted in Figure 17 (colored line segments). Overall, we find that positive trends in sea ice area are significantly weaker in the CESM2 than the CESM1. Over the 600 years examined, there are four 35-year periods in the CESM1 when trends in sea ice area equal or exceed Antarctic sea ice area trends in the satellite observations (0.20×10^6 km^2 increasing sea ice area per decade from 1979 to 2015), an average of one sustained period of increasing sea ice area every 150 years. In the CESM2, on the other hand, there is only one such time period over the entire 600 years examined.

Decreased interannual (and longer time scale) variability in annual mean sea ice area in the CESM2 is also evident when we evaluate persistence in the two models. Figure 18 shows the lagged autocorrelation in annual mean sea ice area, calculated for each model from the full 600-year pre-industrial experiment (solid and dotted black lines denote the lagged autocorrelation in the CESM2 and CESM1, respectively). The decay in the autocorrelation with greater lag follows that of a red noise process in both models, but the e-folding time scale is significantly greater in the CESM1 than the CESM2: the autocorrelation drops below 0.25 in only two years in the CESM2, but requires four years in the CESM1. Therefore, persistence is greater in the CESM1 than the CESM2, hinting at greater predictability in the former than the latter.

We also compare the autocorrelation in sea ice area in the 40-year satellite record (Fig 18, blue lines), which exhibits an even more rapid decline in the lagged correlation

than in the CESM2, and suggests an anti-correlation over certain lags. However, when autocorrelations in the two models are computed over all possible contiguous 40-year intervals in order to sample the model time series in a way more akin to the observations, the observed autocorrelation falls within the range of that in both models. However, the range of the 40-year autocorrelation is somewhat narrower in the CESM2 than the CESM1, particularly with respect to the upper range, which is greater in the CESM1 (Fig 18, shaded grey region is wider than the shaded yellow range).

In Figure 19, we further analyze persistence in sea ice by displaying the autocorrelation of monthly mean sea ice area. As for the annual mean ice area, we find that persistence in monthly ice area is also significantly greater in the CESM1 than the CESM2 (compare Figs 19a and b). Both models show qualitatively similar monthly variations in persistence: the greatest persistence in ice area occurs near the September maximum, and the least persistence occurs at the start of the ice growth season (March in the CESM1 and April to May in the CESM2). However, the e-folding time scale is much longer over most months in the CESM1, compared to the CESM2; while persistence in September ice area is only 6 years in the CESM2, persistence extends to over 20 years in the CESM1.

As expected, we find that decreased persistence in the CESM2 is also accompanied by decreased predictability in this model, relative to the CESM1. Figure 20 shows the correlation between the monthly ice area for a lead month (i.e. the predictor) and for an ensuing lag month (i.e. the predictand), a measure often used to quantify diagnostic predictability (see, e.g., Blanchard-Wrigglesworth et al., 2011). Qualitatively, predictability in each of these models share many general features (though different magnitudes), which have been noted in previous studies of sea ice predictability. In both the CESM2 and CESM1, we find the greatest predictability, which persists over the longest time scales, when the (near-maximum) October sea ice area is the predictor (Blanchard-Wrigglesworth et al., 2011). Conversely, predictability is lowest when early autumn sea ice area is the predictor (Blanchard-Wrigglesworth et al., 2011; M. Holland et al., 2013), though this phasing is slightly different in the two models; predictability is lowest when March and April sea ice area are the predictors in the CESM1, but is lowest when April and May sea ice area are the predictors in the CESM2. Similarly, both models show a decline in predictability of the ice area minimum and the following early growth season (February, March, and April), no matter what month is used as the predictor. However, predictability re-emerges in the following months, likely because ocean mixed layer temperatures

hold the memory of the coupled system over this hiatus period (see Blanchard-Wrigglesworth et al., 2011; M. Holland et al., 2013); ice area is no longer a proxy for the net energy of the coupled ice and ocean mixed layer when large areas of the high-latitude oceans are ice-free and above freezing, as they are at the end of austral summer and early fall (February and March).

Despite these qualitative similarities, Antarctic sea ice area is substantially less predictable in the CESM2 than the CESM1 over nearly all predictor months and predictand time scales (compare Figs 20a and b). In the CESM2, nearly all predictability of the February ice area minimum is lost by the third year (i.e. $r < 0.1$); in the CESM1, on the other hand, predictability of the ice area minimum persists into the fifth year. Similarly, nearly all predictability in the September ice area maximum is lost by the sixth year in the CESM2, but persists into the eighth year and beyond in the CESM1. Such decreased predictability is consistent with decreased persistence in both annual and monthly mean sea ice area in the CESM2, relative to the CESM1.

3.3 Relationships between Sea Ice and Ocean Temperatures

Sea ice is intimately connected to the ocean. The heat content in the ocean mixed layer determines when ice growth commences in autumn, and the maximum thickness and extent that the ice pack attains in winter (Thorndike, 1992; Leppäranta, 1993). Variability in ocean convection can drive variability in sea ice area, as demonstrated by the sizeable sensible heat polyñya that formed over in the Weddell Sea in the 1970s (D. Holland, 2001); similarly, global climate models with multidecadal variability in the strength of the Southern Ocean deep cell also display significant multidecadal variability in Antarctic sea ice area and extent (Martin et al., 2013; Zhang et al., 2019). Even coupling of sea ice to an ocean mixed layer is sufficient to trigger subdecadal to interdecadal (5 to 20 years) variability in ice area and thickness (Bitz et al., 1996).

Furthermore, how the polar oceans respond to a changing climate impacts how the sea ice responds. In a warming world, changes in ocean heat transport into the polar oceans determine the extent of sea ice loss and polar amplification in global climate models (M. Holland & Bitz, 2003; Hwang & Frierson, 2010; Singh et al., 2017). Conversely, initially warmer-than-average Southern Ocean temperatures may be sufficient to drive subsequent ocean cooling and Antarctic sea ice expansion even as the rest of the globe warms due to ris-

ing atmospheric CO_2 (Singh et al., 2019), as has occurred in the Antarctic over much of the satellite era (Parkinson & Cavalieri, 2012).

To discern relationships between variability in upper ocean temperatures and sea ice area in both models, we compute correlations between sea ice area and (monthly and zonal mean) ocean temperatures over the previous twelve months (Figs 21 and 22). For both the February sea ice minimum and the September sea ice maximum, we find strong correlations between ice area and upper ocean temperatures over concurrent and prior months in both the CESM2 and CESM1, which we describe further below.

In both models, the February ice area minimum is negatively correlated with sea surface temperatures (SSTs) and ocean temperatures at 100m depth (Fig 21). Unsurprisingly, warm ocean temperatures (and correspondingly greater upper ocean heat content) are associated with less extensive February ice area, and, conversely, cooler ocean temperatures are associated with more extensive February ice area. Both models also display a number of other shared features in the relationships between ocean temperatures and February sea ice area, though the relationships tend to be of greater magnitude in the CESM1 than the CESM2, possibly reflecting greater persistence in ice area in the former than the latter.

First, both models show greater seasonality in the relationship between SSTs and February ice area, compared to the relationship between 100m temperatures and ice area (compare Figs 21a, b with 21c, d). The weakest relationships between SSTs and sea ice area occur over the middle of the melt season (November and December), which may be due to cold freshwater capping at the sea surface with ice melt at this time of year; such capping shoals the base of the mixed layer and isolates warmer anomalies at depth (M. Holland et al., 2013). Such a weakening of the ocean-ice correlation is not evident at 100m depth. Furthermore, in both models, the relationships between ocean temperatures and ice area are strongest equatorward of the ice edge, and tend to follow the ice edge over the course of the seasonal cycle (Fig 21, compare location of blue regions to black ice edge contour). Conversely, relationships between February ice area and ocean temperatures are weakest under the ice pack, likely because temperatures here remain near freezing for much of the year. Circa February, however, there is a stronger negative correlation between ocean temperatures and ice under the ice pack itself, and this relationship is more robust in the CESM2 than the CESM1; this difference between models may occur be-

cause the February ice pack in the CESM2 is thinner with more open ocean area, compared to that in the CESM1.

Correlations between September sea ice area and ocean temperatures are qualitatively similar to those for February ice area, but are even stronger in magnitude (Fig 22; $r \leq -0.9$ over some latitudes and months). As for February sea ice area, relationships between September sea ice area and ocean temperatures are strongest equatorward of the ice edge, weakest under the ice pack, and exhibit a greater seasonal cycle at the surface than at depth (i.e. for SSTs compared to temperatures at 100m depth; compare Figs 22a, b with c, d). In the CESM2, there are positive correlations between September sea ice area and SSTs under the ice pack, which are not evident in the CESM1. This positive relationship may indicate more upward entrainment of deeper warm anomalies with greater basal ice growth and more brine rejection in the CESM2, since stratification is significantly weaker in this model. Further investigation regarding these relationships is warranted, but outside the scope of the present study.

The strong relationships between sea ice area and ocean temperatures, as shown Figures 21 and 22, suggest that ocean temperatures may be a useful predictor of ice area. However, further examination of these relationships in both models indicates that sea ice area may actually lead ocean temperatures over most latitudes, as gauged by the time of maximum correlation between the two. Figure 23 shows the lead-lag correlations, computed monthly up to a maximum lead-lag of ten years, between (February and September) sea ice area and ocean temperatures at three levels: the surface, 100m depth, and 500m depth. At all levels in both models, the greatest negative correlation between sea ice area and ocean temperatures occurs when sea ice area is the predictor and ocean temperatures are the predictand (i.e. when sea ice area leads), not vice versa (Fig 23, see red markers). Therefore, anomalously extensive sea ice area more strongly leads anomalously cold ocean temperatures than the reverse.

Though ice area appears to lead upper ocean temperatures in both the CESM2 and CESM1, there are some important differences between the two models. First, correlations between ocean temperatures and sea ice area are weaker in the CESM2 than the CESM1, which may reflect decreased persistence in sea ice area in the former than the latter. Furthermore, correlations between sea ice area and ocean temperatures under the ice pack are more often positive in the CESM2 than the CESM1. We hypothesize that

these positive correlations may arise from the more intense seasonal cycle of ice growth in the CESM2 (recall Fig 4), which would promote reduced static stability of the upper ocean (as seen in this model; recall Fig 15), thereby eliciting more upwelling of warm waters from greater depths. More exploration of the physical interactions underlying these strong relationships between ocean and ice is warranted, but lies beyond the scope of the present study.

In Figure 24, we show the lead-lag of the greatest negative correlation between sea ice area and ocean temperatures, by latitude and by ocean depth (at six depths, spanning the surface to 500m). As was also evident from Fig 23, the strongest negative correlations between ocean temperatures at a given depth and sea ice area occurs when sea ice leads ocean temperatures, not vice versa. For both February and September sea ice area, correlations are most negative just beyond the ice edge and at shallower depths (SSTs, 50m, 100m), but are still non-negligible at greater depths. Indeed, ocean temperatures at all latitudes between 60S and 45S (i.e. the ice-free Southern Ocean, beyond the maximum ice edge) appear to follow sea ice area in both models, as gauged the time of maximum negative correlation between the two. This may be due to the climatological ocean circulation at these latitudes, which flows equatorward in the upper ocean due to Ekman transport driven by the surface westerly wind maximum (Marshall & Speer, 2012); as a result, anomalies in ice area may impact ocean temperatures downstream at later times.

Though ocean temperatures appear to follow ice area at most latitudes, we do find some regions where ocean temperatures lead ice area. Under the seasonal ice pack, ocean temperatures appear to lead September ice area by up to five years in both the CESM2 and CESM1 (Figs 24a and b, see markers between vertical green lines). Significant correlations occur for ocean temperatures up to 200m depth, and at latitudes up the continent edge, though relationships are strongest at 100m and near 65S in both models. Relationships are stronger in the CESM1 than the CESM2, as gauged by the magnitude of the correlation. These significant negative correlations between leading ocean temperatures (at depths up to 200m) and lagging September ice area suggest that anomalous heat content in the ocean mixed layer, due to anomalous ocean heat convergence or anomalous summer season heat storage, may offer some measure of predictability of the September sea ice maximum. On the other hand, the greatest negative correlations between ocean temperatures and February sea ice area occur when ice leads ocean (Figs

24c and d), suggesting that ocean temperatures may be a less useful predictor of the sea ice area minimum in these models.

4 Discussion

In this overview of Antarctic sea ice in the new CESM2, we describe its seasonal cycle, interactions with both atmosphere and ocean, interannual persistence, and seasonal-to-interannual predictability relative to that in the CESM1. Overall, we find substantial differences between the old and new models, some of which are attributable to differences in how sea ice thermodynamics is treated, and others that are due to differences in the climatologies of the atmosphere and ocean.

Treating sea ice as a mushy layer, an amalgam with varying amounts of solid ice and microscopic liquid brine inclusions, rather than as a solid with fixed salinity (as in BL99), has been shown to impact the seasonal cycle of sea ice in both hemispheres (A. Turner & Hunke, 2015; Bailey et al., 2020, submitted). We find that in the CESM2, the new mushy-layer thermodynamics treatment changes the spatial and temporal distribution of the different modalities of Antarctic sea ice growth relative to the CESM1. Both frazil (open water) ice formation and snow-to-ice conversion make substantially greater contributions to Antarctic ice growth in the CESM2 than the CESM1, while basal (congelation) growth makes a smaller contribution. Greater frazil ice growth in the CESM2 is concentrated within Antarctic coastal polyñyas, while greater snow-to-ice conversion occurs at the center and edge of the growing ice pack. Observational studies show that such frazil and snow-to-ice growth processes are crucial for Antarctic sea ice growth in the real world (see, e.g., Jeffries et al., 2001; Maqueda et al., 2004; Maksym & Markus, 2008; Tamura et al., 2008), and it is possible that improved representation of these processes in the new model implies better agreement with real-world observations. Further intercomparison between model results and *in situ* observations is needed.

While differing sea ice growth in the CESM2 and CESM1 is attributable in part to the differing sea ice thermodynamic treatments in the two models, differing sea ice thickness and extent are more clearly linked to differing atmosphere and ocean dynamics. The extratropical atmospheric circulation in the Southern Hemisphere is more vigorous in the CESM2 than the CESM1, with more energetic stationary wave activity and surface winds. Deeper subpolar low pressure centers in the CESM2 sweep sea ice away

from the coast (facilitating frazil ice growth in coastal polyñas) increase sea ice divergence from the center of the ice pack, and drive sea ice equatorward. The latter tends to thin the ice pack, which is evident in the climatology of Antarctic sea ice in the CESM2. On the other hand, sea ice area and extent are substantially lower in the CESM2 than the CESM1 as ocean heat flux convergence into the mixed layer is greater in the new model. Greater surface wind stress curl in the CESM2 is responsible for more upwelling of warmer waters from depth, increasing ocean heating under and at the edge of the ice pack; previous studies have shown that such increased ocean heat flux convergence acts as a substantial control on ice extent in Earth system models (Bitz et al., 2005).

While we have attributed differences in sea ice climatology between the CESM2 and CESM1 to the aforementioned factors, decreased Antarctic sea ice persistence and predictability in the new CESM2, relative to the older CESM1, are less readily attributable. There are many differences between the new CESM2 and the older CESM1 that could give rise to the decreased persistence and predictability documented here. One factor of note is the ocean coupling frequency in the CESM2 compared to CESM1: while numerical coupling between the atmosphere and ocean only occurs once per day in the CESM1, it occurs hourly in the CESM2. An increase in coupling frequency may be expected to amplify the influence of atmospheric 'noise' on ocean processes, thereby decreasing their persistence; because sea ice evolution is closely coupled to the ocean, sea ice persistence may also be expected to decrease. As such, more frequent coupling may be expected to impact the signal-to-noise paradox, whereby model experiments seemingly understate the (seasonal, decadal, and multidecadal) predictability of Earth system components because of inadequate dynamical responses (as reviewed by Scaife & Smith, 2018). Whether such greater coupling frequency may decrease persistence and predictability can only be answered by comparing identical model runs with different coupling frequencies, which we reserve for future work.

Decreased Antarctic sea ice persistence in the new CESM2 also has important implications for the gradual expansion in Antarctic sea ice area that occurred over much of the satellite era (1979 to 2015; see Cavalieri et al., 1996, updated yearly). As neither stratospheric ozone loss (Sigmond & Fyfe, 2010; Bitz & Polvani, 2012; Landrum et al., 2017) nor freshwater forcing (Swart & Fyfe, 2013; Pauling et al., 2016) appear to explain observed Antarctic sea ice expansion, internal variability has been proposed as the simplest explanation for the observations (Polvani & Smith, 2013; Zhang et al., 2019; Singh

et al., 2019). While many climate models commonly display multidecadal sea ice area expansion in their pre-industrial control runs similar to that in the satellite observations (Polvani & Smith, 2013), the CESM2 only does so very infrequently. Antarctic sea ice expansion over the observational period could be attributable to internal variability, forced change, or a combination of the two. The differences in low frequency variability across models shown here suggests that there are considerable challenges in using models to quantify these potential factors. That sea ice area trends in the CESM2 are less persistent than those documented in other models suggests that further measures of persistence in the real-world or from theory would be useful for constraining sea ice variability in GCMs.

Finally, we have also shown that in both the CESM2 and CESM1, sea ice area and Southern Ocean temperatures (above 500m) are highly correlated, albeit less strongly in the CESM2 than in the CESM1. While upper ocean temperatures under the seasonal icepack appear to lead the September sea ice maximum, temperatures in the open Southern Ocean appear to follow both September and February sea ice area. Though seemingly unintuitive, these relationships are consistent with the prevailing general circulation over the Southern Ocean, where westerly surface winds over the Southern Ocean drive sea ice, and related upper ocean anomalies, northwards. As such, temperature anomalies over the open Southern Ocean would be expected to follow more southerly anomalies, some of which may be related to sea ice. Further in-depth, month-by-month analysis of these relationships between sea ice area and upper ocean temperature would help improve understanding of the coupled evolution of the upper ocean and sea ice in the Antarctic region.

In this overview of Antarctic sea ice in the state-of-the-art CESM2, we have highlighted key differences in sea ice climatology and variability between the older CESM1 and the newer model. As Antarctic sea ice begins to retreat in response to a warming climate, Earth system models will continue to be an important tool for understanding the changing interplay between sea ice, ocean, and atmosphere in a warming world. The CESM2, in conjunction with observations, reanalyses, and other Earth system models, will serve as an indispensable resource for understanding and anticipating these changes in Antarctic climate in the future.

Acknowledgments

The CESM2 model output used in this study is available at the NCAR Digital Asset Services Hub (DASH; https://data.ucar.edu); the CESM1 model output is available at the CESM Large Ensemble Community Project site (http://www.cesm.ucar.edu/projects/community-projects/LENS/). The CESM project is supported primarily by the National Science Foundation (NSF). This material is based upon work supported by the National Center for Atmospheric Research (NCAR), which is a major facility sponsored by the NSF under Cooperative Agreement No. 1852977. Computing and data storage resources, including the Cheyenne supercomputer (doi:10.5065/D6RX99HX), were provided by the Computational and Information Systems Laboratory (CISL) at NCAR. LL was funded by NSF grant 1643484.

References

Andreas, E., & Ackley, S. (1982). On the differences in ablation seasons of arctic and antarctic sea ice. *Journal of the Atmospheric Sciences*, *39*(2), 440–447.

Armour, K., Marshall, J., Scott, J., Donohoe, A., & Newsom, E. (2016, Jul). Southern Ocean warming delayed by circumpolar upwelling and equatorward transport. *Nature Geoscience*, *9*, 549-554.

Bailey, D., Holland, M., DuVivier, A., Hunke, E., & Turner, A. (2020, submitted). Impact of sea ice thermodynamics in the CESM2 sea ice component. *Journal of Advances in Modeling Earth Systems*.

Beljaars, A., Brown, A., & Wood, N. (2004). A new parametrization of turbulent orographic form drag. *Quarterly Journal of the Royal Meteorological Society*, *130*(599), 1327–1347.

Bintanja, R., van Oldenborgh, G., Drijfhout, S. S., Wouters, B., & Katsman, C. (2013, Jul). Important role for ocean warming and increased ice-shelf melt in Antarctic sea ice expansion. *Nature Geoscience*, *6*, 376-379.

Bitz, C., Battisti, D., Moritz, R., & Beesley, J. (1996). Low-frequency variability in the Arctic atmosphere, sea ice, and upper-ocean climate system. *Journal of Climate*, *9*(2), 394-408.

Bitz, C., Holland, M., Hunke, E., & Moritz, R. (2005, Aug). Maintenance of the sea ice edge. *Journal of Climate*, *18*, 2903-2921.

Bitz, C., & Lipscomb, W. (1999). An energy-conserving thermodynamic model of

sea ice. *Journal of Geophysical Research: Oceans*, *104*(C7), 15669–15677.

Bitz, C., & Polvani, L. (2012). Antarctic climate response to stratospheric ozone depletion in a fine resolution ocean climate model. *Geophysical Research Letters*, *39*(L20705).

Bitz, C., Shell, K., Gent, P., Bailey, D., Danabasoglu, G., Armour, K., ... Kiehl, J. (2012). Climate sensitivity in the Community Climate System Model, version 4. *Journal of Climate*, *25*(9), 3053-70.

Blackport, R., & Kushner, P. (2017). Isolating the atmospheric circulation response to arctic sea ice loss in the coupled climate system. *Journal of Climate*, *30*(6), 2163–2185.

Blanchard-Wrigglesworth, E., Armour, K., Bitz, C., & DeWeaver, E. (2011). Persistence and inherent predictability of arctic sea ice in a gcm ensemble and observations. *Journal of Climate*, *24*(1), 231–250.

Bogenschutz, P., Gettelman, A., Hannay, C., Larson, V., Neale, R., Craig, C., & Chen, C.-C. (2018). The path to cam6: Coupled simulations with cam5. 4 and cam5. 5. *Geoscientific Model Development (Online)*, *11*(LLNL-JRNL-731418).

Cavalieri, D., Parkinson, C., Gloersen, P., Comiso, J., & Zwally, H. (1999). Deriving long-term time series of sea ice cover from satellite passive-microwave multisensor data sets. *Journal of Geophysical Research: Oceans*, *104*(C7), 15803–15814.

Cavalieri, D., Parkinson, C., Gloersen, P., & Zwally, H. (1996, updated yearly). *Sea ice concentrations from Nimbus-7 SMMR and DMSP SSM/I-SSMIS passive microwave data, version 1.* NASA National Snow and Ice Data Center Distributed Archive Center.

Comiso, J., & Nishio, F. (2008). Trends in the sea ice cover using enhanced and compatible amsr-e, ssm/i, and smmr data. *Journal of Geophysical Research: Oceans*, *113*(C2).

Danabasoglu, G., Lamarque, J.-F., Bacmeister, J., Bailey, D., DuVivier, A., Edwards, J., ... others (2019). The community earth system model version 2 (cesm2). *Journal of Advances in Modeling Earth Systems*.

Deser, C., Tomas, R., & Sun, L. (2015, Mar). The role of ocean-atmosphere coupling in the zonal-mean atmospheric response to Arctic sea ice loss. *Journal of Climate*, *28*, 2168-2186.

DuVivier, A., Holland, M., Kay, J., Tilmes, S., Gettelman, A., & Bailey, D. (2019, submitted). Arctic and antarctic sea ice state in the community earth system model version 2. *Journal of Geophysical Research: Oceans*.

Eicken, H. (2003). Sea ice: an introduction to its physics, chemistry, biology and geology. In (p. 22-81). Wiley Online Library.

Eicken, H., Fischer, H., & Lemke, P. (1995). Effects of the snow cover on antarctic sea ice and potential modulation of its response to climate change. *Annals of Glaciology*, *21*, 369–376.

England, M., Polvani, L., & Sun, L. (2018). Contrasting the antarctic and arctic atmospheric responses to projected sea ice loss in the late twenty-first century. *Journal of Climate*, *31*(16), 6353–6370.

Feltham, D., Untersteiner, N., Wettlaufer, J., & Worster, M. (2006). Sea ice is a mushy layer. *Geophysical Research Letters*, *33*(14).

Garrison, D., & Buck, K. (1989). The biota of antarctic pack ice in the weddell sea and antarctic peninsula regions. *Polar Biology*, *10*(3), 211–219.

Gettelman, A., & Morrison, H. (2015). Advanced two-moment bulk microphysics for global models. part i: Off-line tests and comparison with other schemes. *Journal of Climate*, *28*(3), 1268–1287.

Gettelman, A., Morrison, H., Santos, S., Bogenschutz, P., & Caldwell, P. (2015). Advanced two-moment bulk microphysics for global models. part ii: Global model solutions and aerosol–cloud interactions. *Journal of Climate*, *28*(3), 1288–1307.

Goosse, H., Campin, J.-M., Fichefet, T., & Deleersnijder, E. (1997). Impact of sea-ice formation on the properties of antarctic bottom water. *Annals of Glaciology*, *25*, 276–281.

Gordon, A. (1981). Seasonality of southern ocean sea ice. *Journal of Geophysical Research: Oceans*, *86*(C5), 4193–4197.

Guo, H., Golaz, J.-C., Donner, L., Wyman, B., Zhao, M., & Ginoux, P. (2015). Clubb as a unified cloud parameterization: Opportunities and challenges. *Geophysical Research Letters*, *42*(11), 4540–4547.

Holland, D. (2001). Explaining the weddell polynya–a large ocean eddy shed at maud rise. *Science*, *292*(5522), 1697–1700.

Holland, M., & Bitz, C. (2003). Polar amplification of climate change in coupled

models. *Climate Dynamics*, *21*, 221-232.

Holland, M., Blanchard-Wrigglesworth, E., Kay, J., & Vavrus, S. (2013). Initial-value predictability of antarctic sea ice in the community climate system model 3. *Geophysical Research Letters*, *40*(10), 2121–2124.

Holland, M., Landrum, L., Kostov, Y., & Marshall, J. (2017). Sensitivity of Antarctic sea ice to the Southern Annular Mode in coupled climate models. *Climate Dynamics*, *49*, 1813-1831.

Holland, M., Landrum, L., Raphael, M., & Kwok, R. (2018). The regional, seasonal, and lagged influence of the amundsen sea low on antarctic sea ice. *Geophysical Research Letters*, *45*(20), 11–227.

Hoose, C., Kristjánsson, J., Chen, J.-P., & Hazra, A. (2010). A classical-theory-based parameterization of heterogeneous ice nucleation by mineral dust, soot, and biological particles in a global climate model. *Journal of the Atmospheric Sciences*, *67*(8), 2483–2503.

Hunke, E., & Lipscomb, W. (2008). *CICE: the Los Alamos sea ice model, documentation and software, version 4.0* (Tech. Rep. No. LA-CC-06-012). Los Alamos National Laboratory.

Hunke, E., Lipscomb, W., Turner, A., Jeffery, N., & Elliott, S. (2015). *CICE: the Los Alamos sea ice model, documentation and software, version 5.1* (Tech. Rep. No. LA-CC-06-012). T-E Fluid Dynamics Group, Los Alamos National Laboratory.

Hwang, Y.-T., & Frierson, D. (2010). Increasing atmospheric poleward energy transport with global warming. *Geophysical Research Letters*, *37*(L24807), 1-5.

Jeffries, M., Krouse, H., Hurst-Cushing, B., & Maksym, T. (2001). Snow-ice accretion and snow-cover depletion on antarctic first-year sea-ice floes. *Annals of Glaciology*, *33*, 51–60.

Kay, J., Deser, C., Phillips, A., Mai, A., Hannay, C., Strand, G., ... Vertenstein, M. (2015). The Community Earth System Model (CESM) Large Ensemble project: A community resource for studying climate change in the presence of internal climate variability. *Bulletin of the American Meteorological Society*, *96*, 1333-1349.

Kwok, R., & Comiso, J. (2002). Southern ocean climate and sea ice anomalies associated with the southern oscillation. *Journal of Climate*, *15*(5), 487–501.

Landrum, L., Holland, M., Raphael, M., & Polvani, L. (2017). Stratospheric ozone depletion: An unlikely driver of the regional trends in antarctic sea ice in austral fall in the late twentieth century. *Geophysical Research Letters*, *44*(21), 11–062.

Larson, V. (2017). Clubb-silhs: A parameterization of subgrid variability in the atmosphere. *arXiv preprint arXiv:1711.03675*.

Leppäranta, M. (1993). A review of analytical models of sea-ice growth. *Atmosphere-Ocean*, *31*(1), 123–138.

Maksym, T., & Markus, T. (2008). Antarctic sea ice thickness and snow-to-ice conversion from atmospheric reanalysis and passive microwave snow depth. *Journal of Geophysical Research: Oceans*, *113*(C2).

Maqueda, M. M., Willmott, A., & Biggs, N. (2004). Polynya dynamics: A review of observations and modeling. *Reviews of Geophysics*, *42*(1).

Marshall, J., & Speer, K. (2012). Closure of the meridional overturning circulation through southern ocean upwelling. *Nature Geoscience*, *5*(3), 171–180.

Martin, T., Park, W., & Latif, M. (2013). Multi-centennial variability controlled by Southern Ocean convection in the Kiel Climate Model. *Climate Dynamics*, *40*, 2005-2022.

Massom, R., Eicken, H., Hass, C., Jeffries, M., Drinkwater, M., Sturm, M., ... others (2001). Snow on antarctic sea ice. *Reviews of Geophysics*, *39*(3), 413–445.

Massom, R., Scambos, T., Bennetts, L., Reid, P., Squire, V., & Stammerjohn, S. (2018). Antarctic ice shelf disintegration triggered by sea ice loss and ocean swell. *Nature*, *558*(7710), 383–389.

Maykut, G., & Untersteiner, N. (1971). Some results from a time-dependent thermodynamic model of sea ice. *Journal of Geophysical Research*, *76*(6), 1550–1575.

McGraw, M., & Barnes, E. (2016). Seasonal sensitivity of the eddy-driven jet to tropospheric heating in an idealized AGCM. *Journal of Climate*, *29*, 5223-5240.

Meehl, G., Arblaster, J., Bitz, C., Chung, C., & Teng, H. (2016). Antarctic sea-ice expansion between 2000 and 2014 driven by tropical pacific decadal climate variability. *Nature Geoscience*, *9*(8), 590–595.

Ohshima, K., Fukamachi, Y., Williams, G., Nihashi, S., Roquet, F., Kitade, Y., ... others (2013). Antarctic bottom water production by intense sea-ice formation in the cape darnley polynya. *Nature Geoscience*, *6*(3), 235–240.

Parkinson, C., & Cavalieri, D. (2012). Antarctic sea ice variability and trends, 1979-2010. *The Cryosphere*, *6*, 871-880.

Pauling, A., Bitz, C., Smith, I., & Langhorne, P. (2016). The response of the Southern Ocean and Antarctic sea ice to freshwater from ice shelves in an Earth System Model. *Journal of Climate*, *29*, 1655-1672.

Pellichero, V., Sallée, J.-B., Schmidtko, S., Roquet, F., & Charrassin, J.-B. (2017). The ocean mixed layer under southern ocean sea-ice: Seasonal cycle and forcing. *Journal of Geophysical Research: Oceans*, *122*(2), 1608–1633.

Perovich, D., Richter-Menge, J., Polashenski, C., Elder, B., Arbetter, T., & Brennick, O. (2014). Sea ice mass balance observations from the north pole environmental observatory. *Geophysical Research Letters*, *41*(6), 2019–2025.

Polvani, L., & Smith, K. (2013). Can natural variability explain observed Antarctic sea ice trends? new modeling evidence from CMIP5. *Geophysical Research Letters*, *40*, 3195-3199.

Powell, D., Markus, T., & Stössel, A. (2005). Effects of snow depth forcing on southern ocean sea ice simulations. *Journal of Geophysical Research: Oceans*, *110*(C6).

Raphael, M. (2004). A zonal wave 3 index for the southern hemisphere. *Geophysical Research Letters*, *31*(23).

Raphael, M. (2007). The influence of atmospheric zonal wave three on antarctic sea ice variability. *Journal of Geophysical Research: Atmospheres*, *112*(D12).

Raphael, M., & Hobbs, W. (2014). The influence of the large-scale atmospheric circulation on antarctic sea ice during ice advance and retreat seasons. *Geophysical Research Letters*, *41*(14), 5037–5045.

Rothrock, D., Yu, Y., & Maykut, G. (1999). Thinning of the arctic sea-ice cover. *Geophysical Research Letters*, *26*(23), 3469–3472.

Scaife, A., & Smith, D. (2018). A signal-to-noise paradox in climate science. *npj Climate and Atmospheric Science*, *1*(1), 1–8.

Scinocca, J., & McFarlane, N. (2000). The parametrization of drag induced by stratified flow over anisotropic orography. *Quarterly Journal of the Royal Meteorological Society*, *126*(568), 2353–2393.

Shi, X., Liu, X., & Zhang, K. (2015). Effects of pre-existing ice crystals on cirrus clouds and comparison between different ice nucleation parameterizations with

the community atmosphere model (cam5). *Atmospheric Chemistry and Physics (Online)*, *15*(PNNL-SA-103838).

Sigmond, M., & Fyfe, J. (2010). Has the ozone hole contributed to increased Antarctic sea ice extent? *Geophysical Research Letters*, *37*(L18502).

Simpkins, G., Ciasto, L., Thompson, D., & England, M. (2012). Seasonal relationships between large-scale climate variability and antarctic sea ice concentration. *Journal of Climate*, *25*(16), 5451–5469.

Singh, H., Garuba, O., & Rasch, P. (2018). How asymmetries between Arctic and Antarctic climate sensitivity are modified by the ocean. *Geophysical Research Letters*, *45*(23), 13-31.

Singh, H., Polvani, L., & Rasch, P. (2019). Antarctic sea ice expansion, driven by internal variability, in the presence of increasing atmospheric co2. *Geophysical Research Letters*(doi: 10.1029/2019GL083758).

Singh, H., Rasch, P., & Rose, B. (2017). Increased ocean heat transports into the high latitudes with co_2-doubling enhance polar-amplified warming. *Geophysical Research Letters*.

Smith, D., Dunstone, N., Scaife, A., Fiedler, E., Copsey, D., & Hardiman, S. (2017). Atmospheric response to arctic and antarctic sea ice: The importance of ocean–atmosphere coupling and the background state. *Journal of Climate*, *30*(12), 4547–4565.

Swart, N., & Fyfe, J. (2013). The influence of recent Antarctic ice sheet retreat on simulated sea ice area trends. *Geophysical Research Letters*, *40*, 4328-4332.

Swart, N., Fyfe, J., Hawkins, E., Kay, J., & Jahn, A. (2015). Influence of internal variability on arctic sea-ice trends. *Nature Climate Change*, *5*(2), 86.

Tamura, T., Ohshima, K., & Nihashi, S. (2008). Mapping of sea ice production for antarctic coastal polynyas. *Geophysical Research Letters*, *35*(7).

Thorndike, A. (1992). A toy model linking atmospheric thermal radiation and sea ice growth. *Journal of Geophysical Research*, *97*(C6), 9401-9410.

Turner, A., & Hunke, E. (2015). Impacts of a mushy-layer thermodynamic approach in global sea-ice simulations using the cice sea-ice model. *Journal of Geophysical Research: Oceans*, *120*(2), 1253–1275.

Turner, A., Hunke, E., & Bitz, C. (2013). Two modes of sea-ice gravity drainage: A parameterization for large-scale modeling. *Journal of Geophysical Research:*

Oceans, *118*(5), 2279–2294.

Turner, J., Comiso, J., Marshall, G., Lachlan-Cope, T., Bracegirdle, T., Maksym, T., ... Orr, A. (2009). Non-annular atmospheric circulation change induced by stratospheric ozone depletion and its role in the recent increase in Antarctic sea ice extent. *Geophysical Research Letters*, *36*(L08502).

Vancoppenolle, M., Fichefet, T., & Goosse, H. (2009). Simulating the mass balance and salinity of arctic and antarctic sea ice. 2. importance of sea ice salinity variations. *Ocean Modelling*, *27*(1-2), 54–69.

Wall, C., Kohyama, T., & Hartmann, D. (2017). Low-cloud, boundary layer, and sea ice interactions over the Southern Ocean during winter. *Journal of Climate*, *30*, 4857-4871.

Wang, Y., Liu, X., Hoose, C., & Wang, B. (2014). Different contact angle distributions for heterogeneous ice nucleation in the community atmospheric model version 5. *Atmospheric Chemistry and Physics*, *14*(19), 10411–10411.

Worby, A., Geiger, C., Paget, M., Woert, M. V., Ackley, S., & DeLiberty, T. (2008). Thickness distribution of antarctic sea ice. *Journal of Geophysical Research: Oceans*, *113*(C5).

Zhang, L., Delworth, T., Cooke, W., & Yang, X. (2019). Natural variability of Southern Ocean convection as a driver of observed climate trends. *Nature Climate Change*, *9*(1), 59.

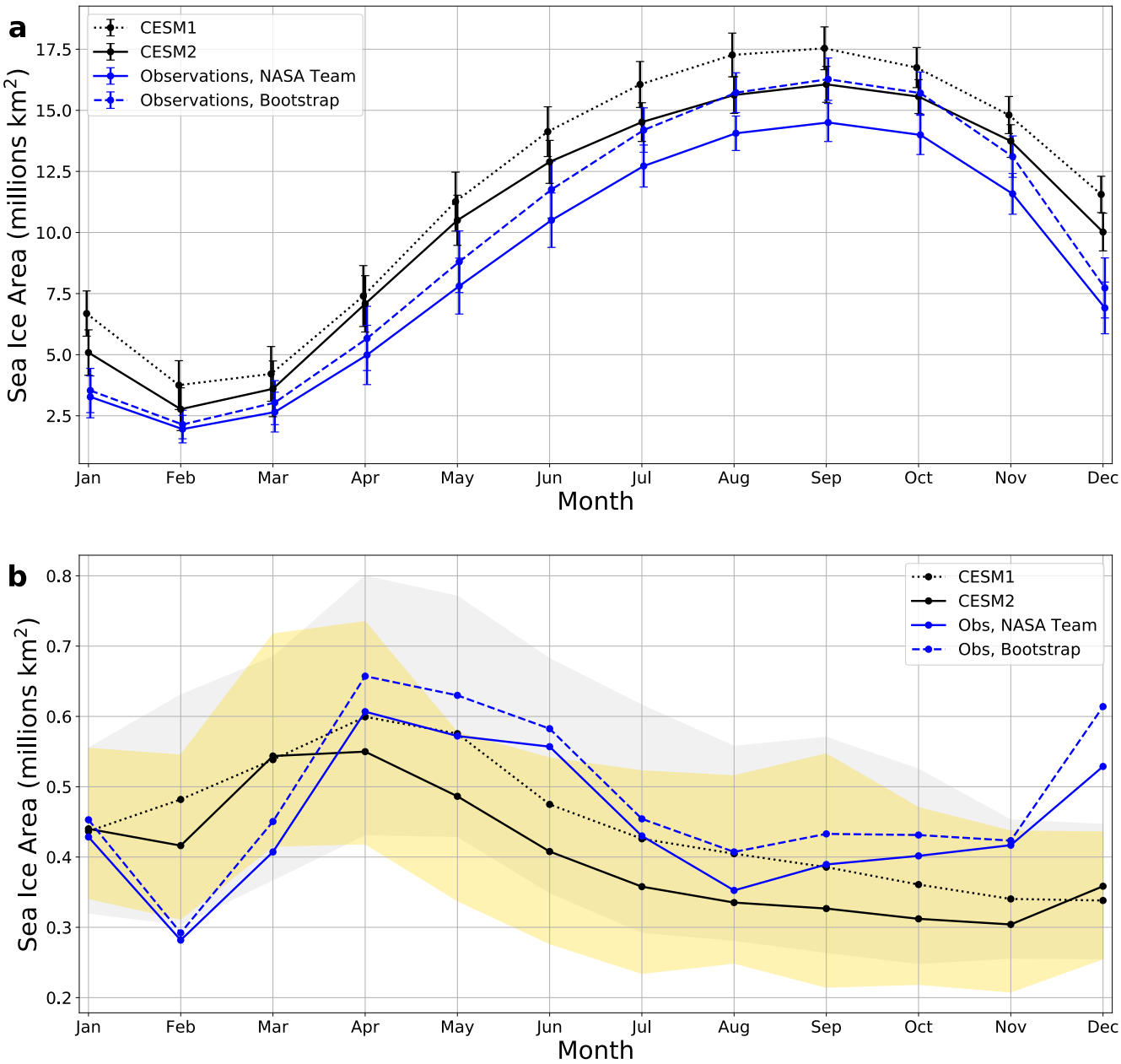

Figure 1. Seasonal Cycle of Sea Ice Area: (a) Monthly mean sea ice area, and (b) one standard deviation of the monthly sea ice area, both in 10^6 km^2. Shown for the CESM2 (black, solid), CESM1 (black, dotted), and the satellite observations from 1979 to 2018 (blue). Range bars in (a) provide the two standard deviation envelope for the variability in monthly ice area, while the yellow and grey shading in (b) give the range of the 40-yr standard deviation from the CESM2 and CESM1, respectively.

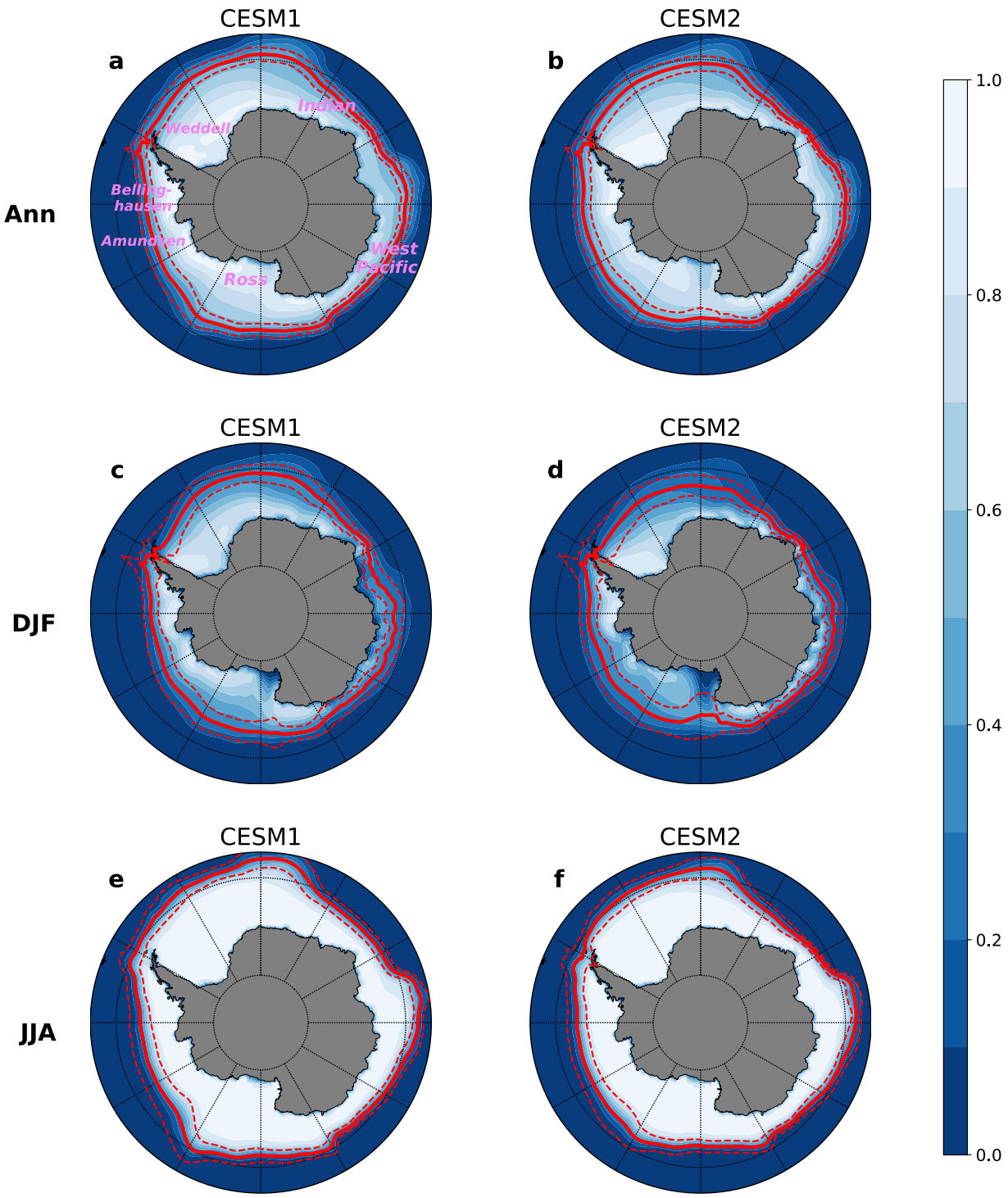

Figure 2. Ice Fraction and Extent: Sea ice fraction (colors) and sea ice extent (the 0.15 ice fraction isoline; thick red contour) in the (a, c, e) CESM1 and (b, d, f) CESM2 in (a, b) the annual mean, (c, d) the December-January-February (DJF) mean, and (e, f) the June-July-Auguest (JJA) mean. In all panels, the dashed red contours show the one-standard-deviation envelope of the ice extent. Panel a indicates the sectors of the Antarctic referred to in the main text.

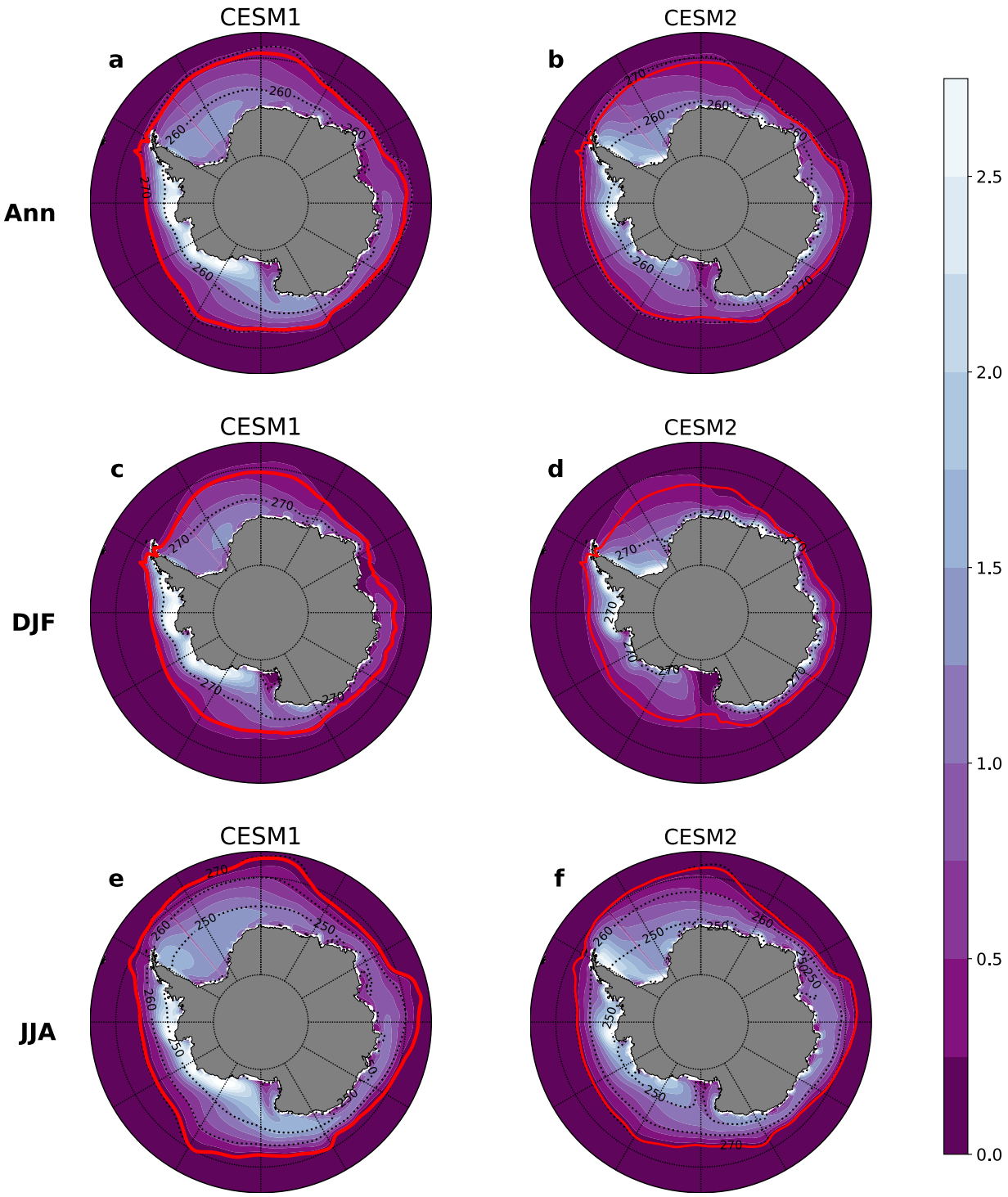

Figure 3. Ice Thickness and Surface Temperature: Sea ice thickness (in m; colors) and surface temperature (dotted contours at 250, 260, 270 K) in the (a, c, e) CESM1 and (b, d, f) CESM2 in (a, b) the annual mean, (c, d) the December-January-February (DJF) mean, and (e, f) the June-July-Auguest (JJA) mean. In all panels, the red contour shows the 0.15 ice fraction isoline.

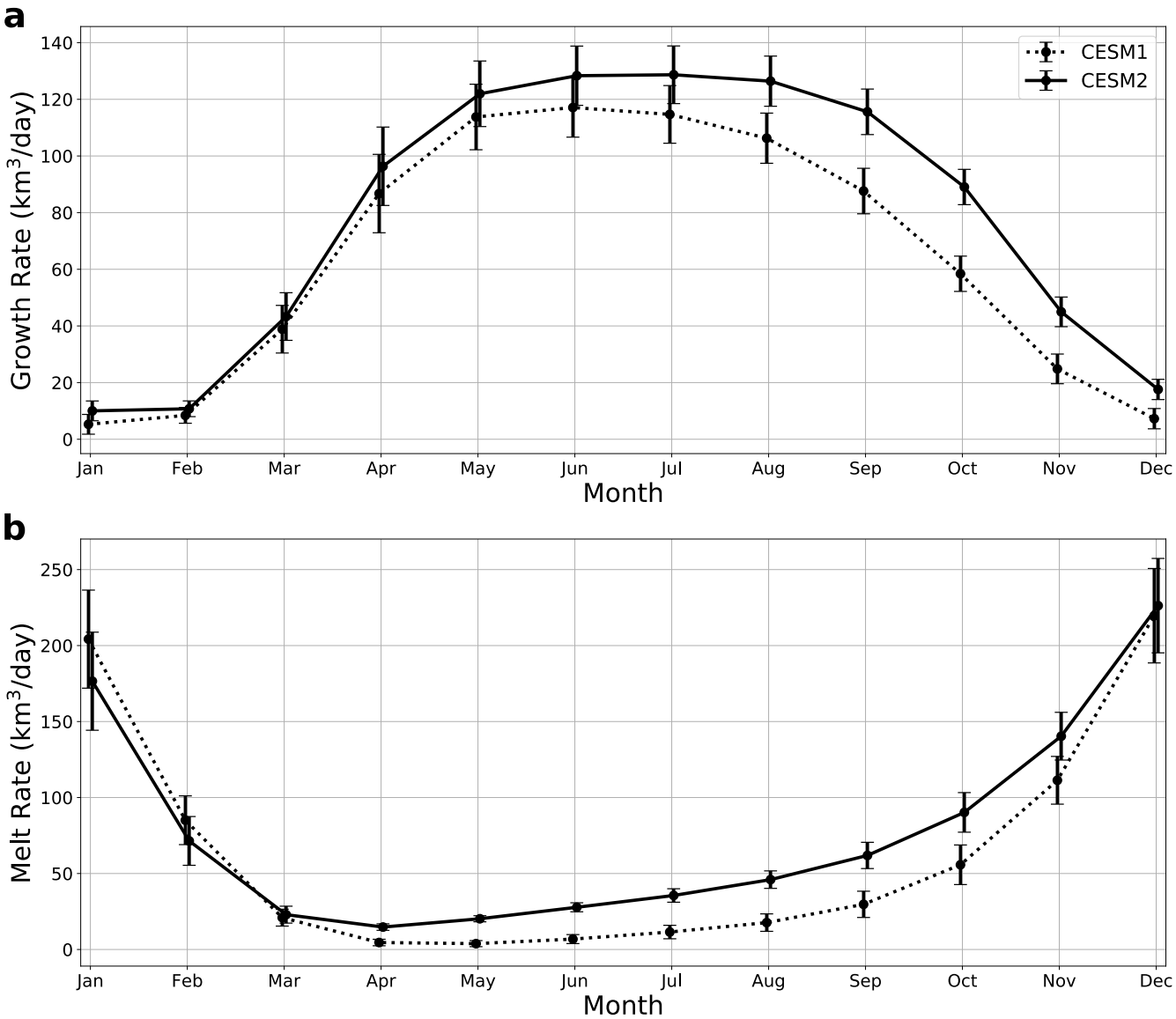

Figure 4. Antarctic Sea Ice Growth and Melt Rates: Monthly mean total sea ice (a) growth rate and (b) melt rate over the Antarctic in the CESM2 (solid line) and the CESM1 (dotted line), in km^3/day. Error bars show the one-standard-deviation range for each month and each model.

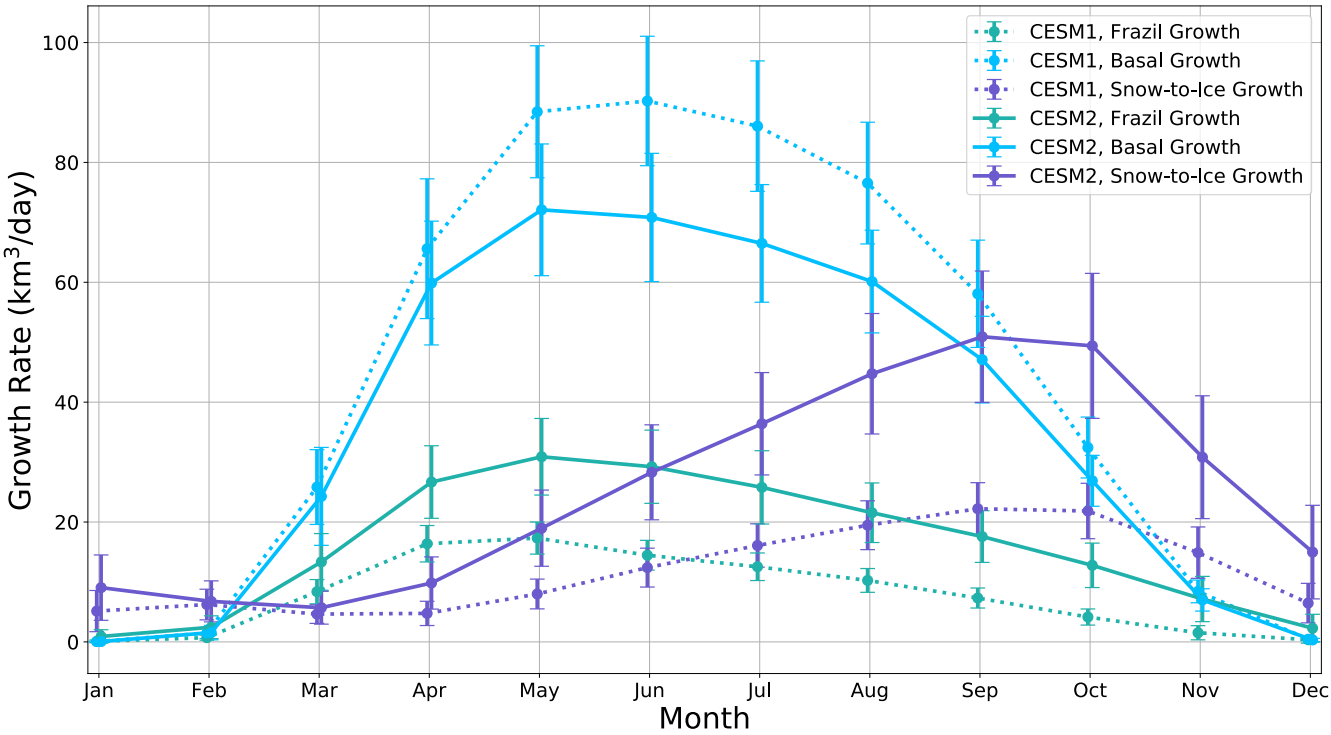

Figure 5. Components of Antarctic Sea Ice Growth: Monthly mean frazil growth (teal lines), basal growth (turquoise lines), and snow-to-ice growth (purple lines) in the CESM2 (solid lines) and CESM1 (dotted lines), in km^3/day. Error bars show the one-standard-deviation range for each month and each model.

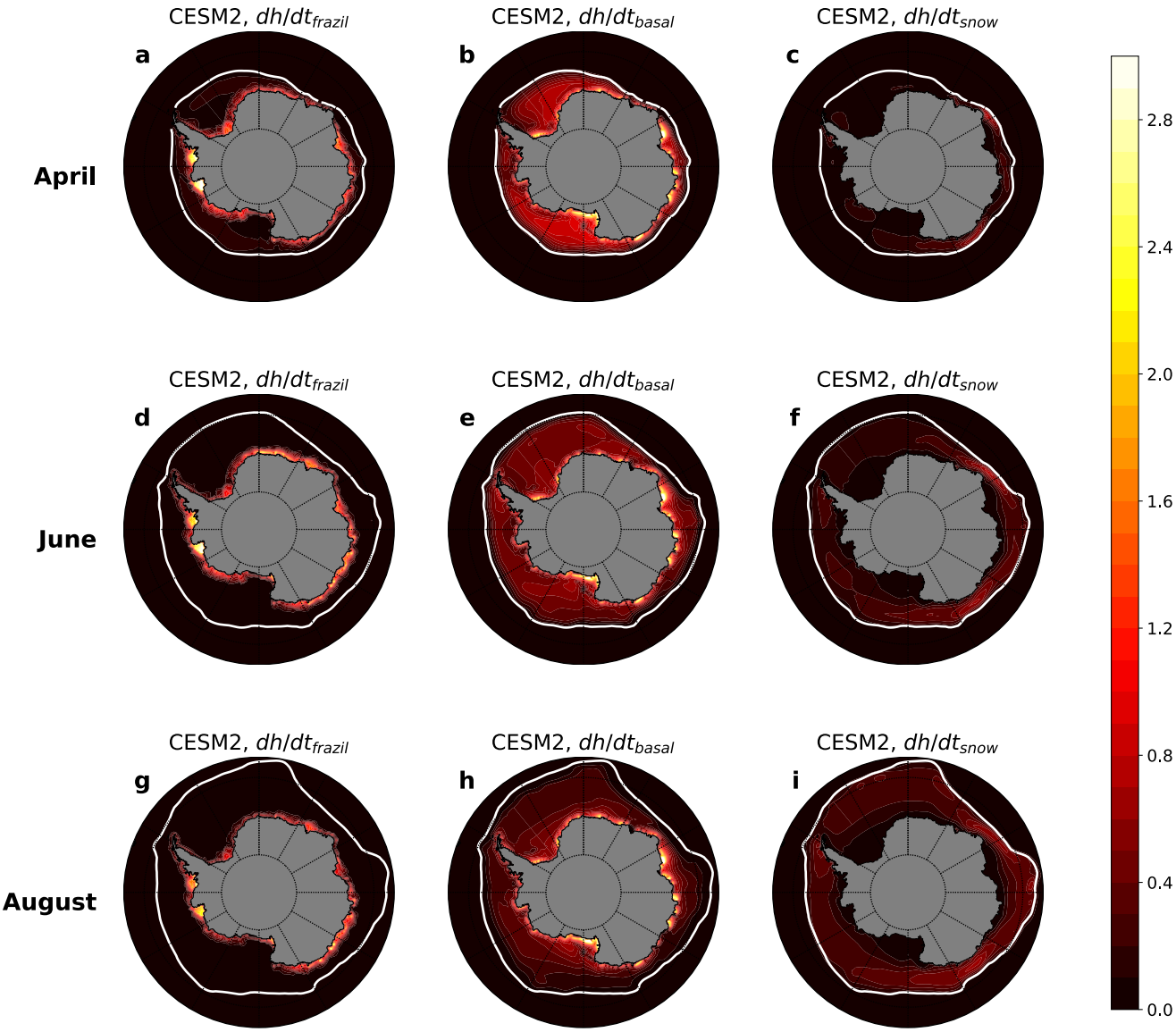

Figure 6. Antarctic Sea Ice Growth in the CESM2: Monthly mean (a, d, g) frazil growth, (b, e, h) basal growth, and (c, f, i) snow-to-ice growth in (a, b, c) April, (d, e, f) June, and (g, h, i) August, in cm/day. In all panels, the white contour shows the 0.15 ice fraction isoline.

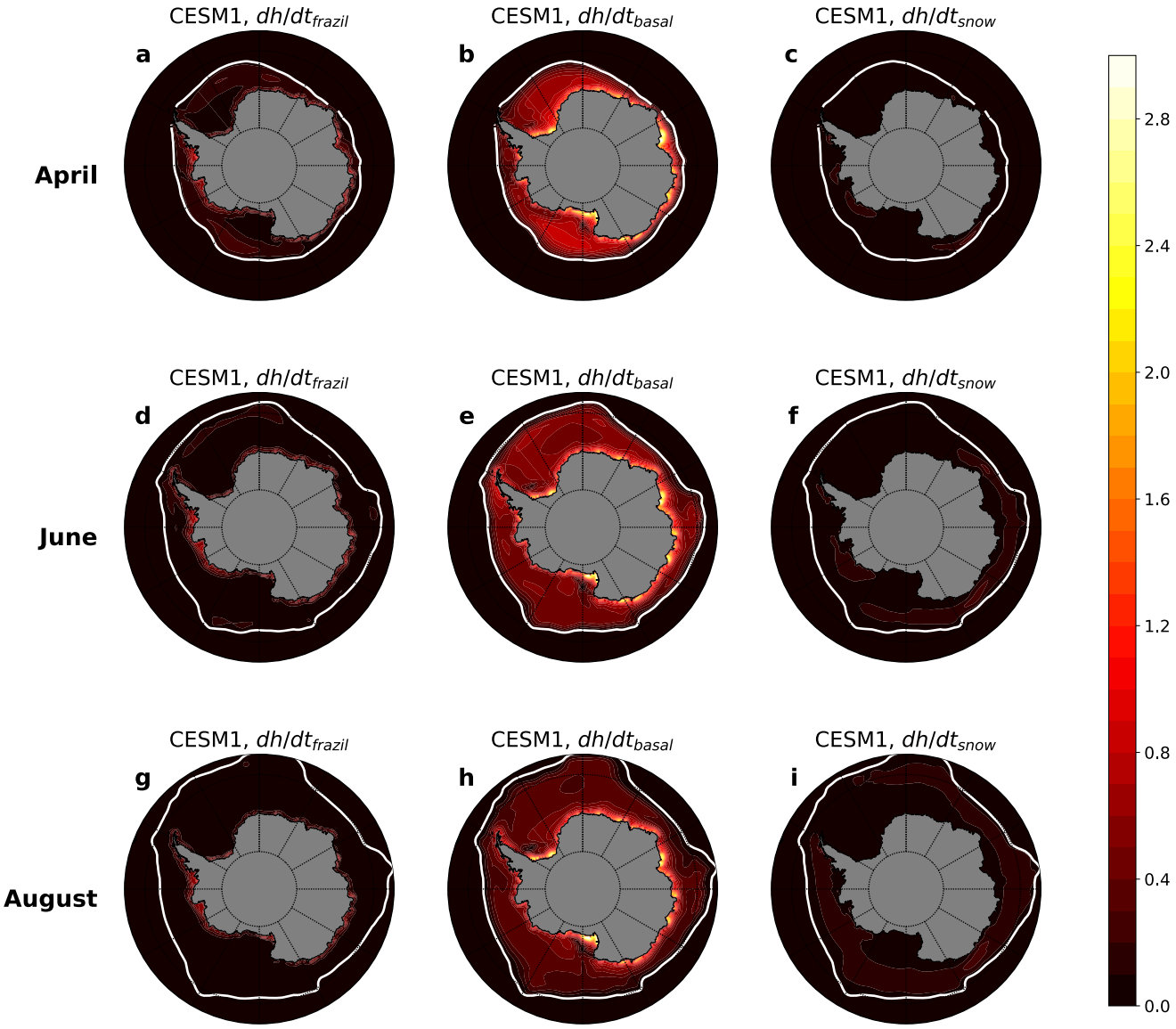

Figure 7. Antarctic Sea Ice Growth in the CESM1: As in Fig 6, but for the CESM1.

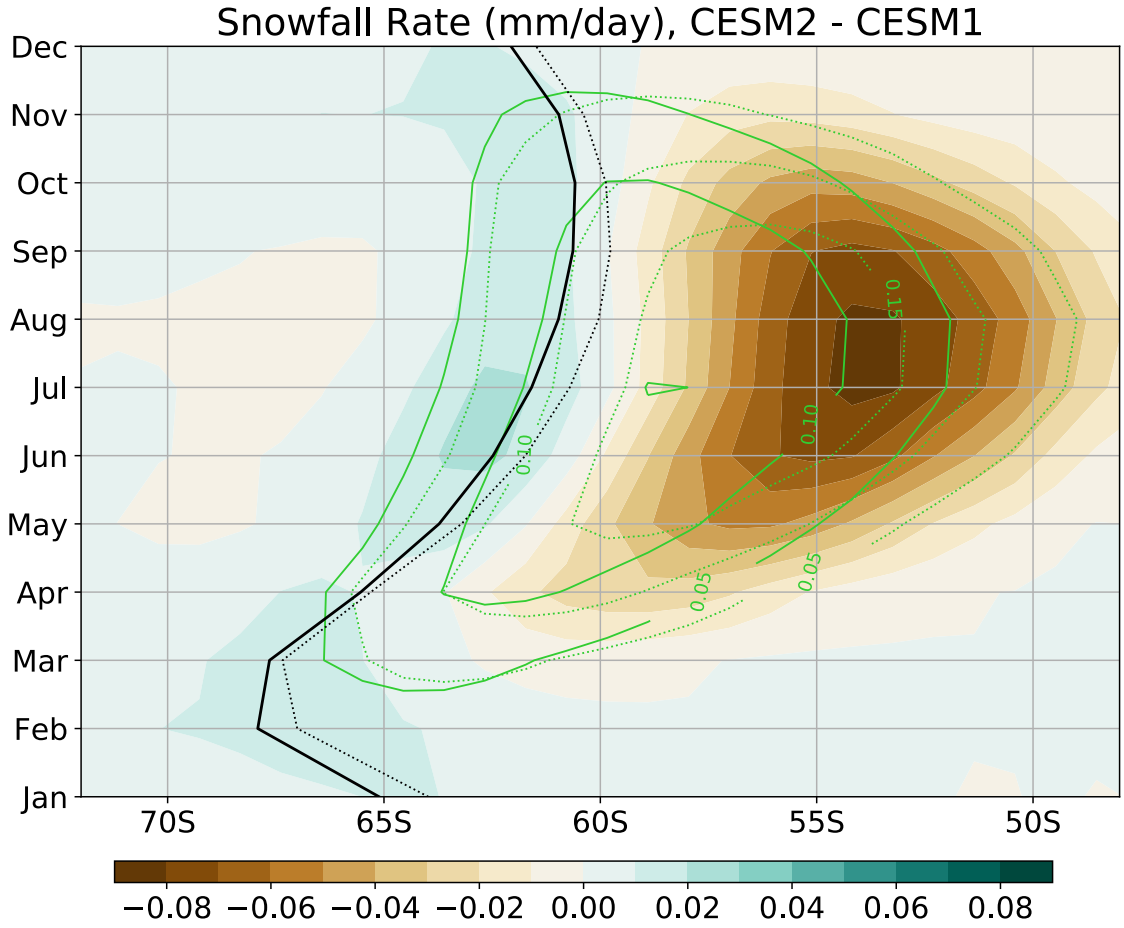

Figure 8. Zonal Mean Monthly Snowfall Rate: Difference between the monthly zonal mean snowfall rate in the CESM2 and CESM1 (in mm/day; colors). Green solid and dotted contours (at 0.05, 0.1, and 0.15 mm/day) show the monthly zonal mean snowfall rates in the CESM2 and CESM1, respectively. The monthly zonal mean ice extent (0.15 ice fraction isoline) for the CESM2 (CESM1) is indicated by the solid (dotted) black contour.

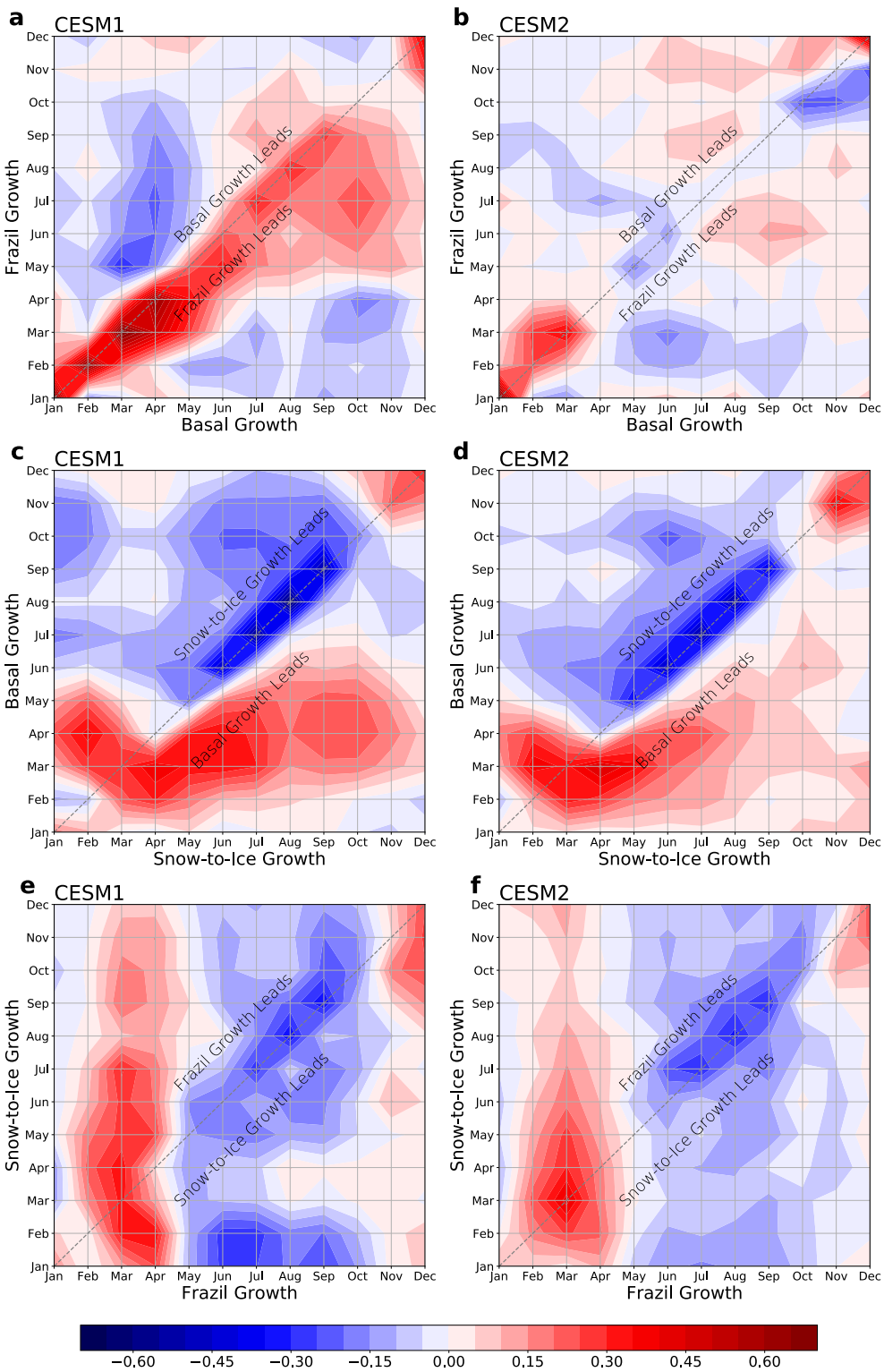

Figure 9. Relationships Between Sea Ice Growth Terms: Monthly lead-lag correlations between (a, b) frazil and basal growth, (c, d) basal and snow-to-ice growth, and (e, f) snow-to-ice and frazil growth in the (a, c, e) CESM1 and (b, d, f) CESM2.

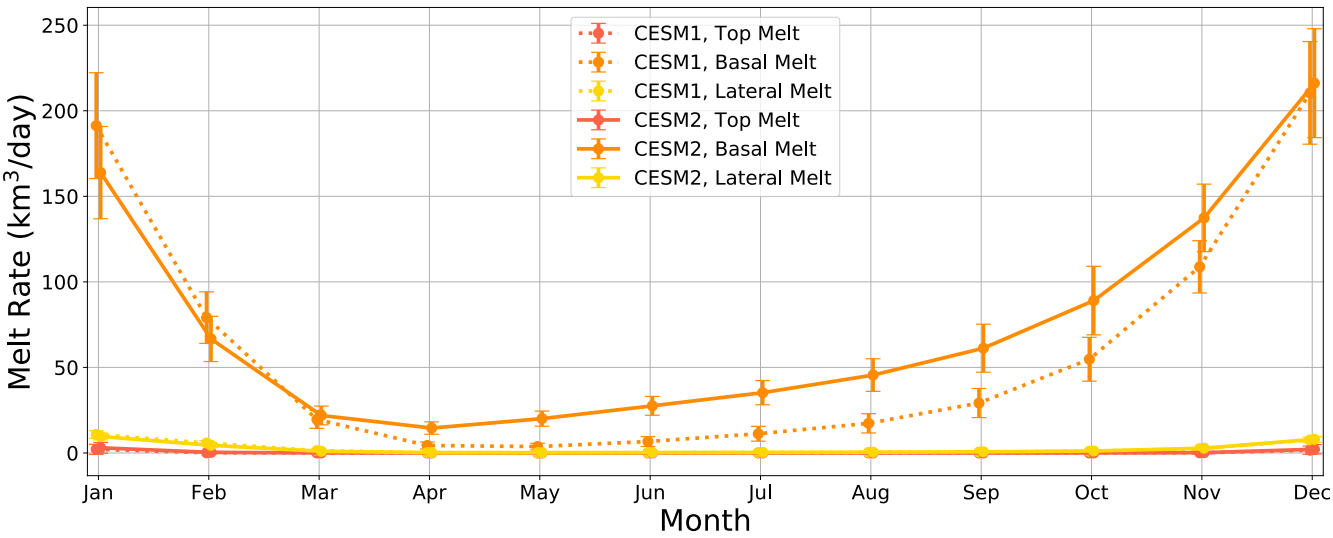

Figure 10. Components of Antarctic Sea Ice Melt: Monthly mean basal melt (orange lines), lateral melt (goldenrod lines), and top melt (red lines) in the CESM2 (solid lines) and CESM1 (dotted lines), in km^3/day. Error bars show the one-standard-deviation range for each month and each model.

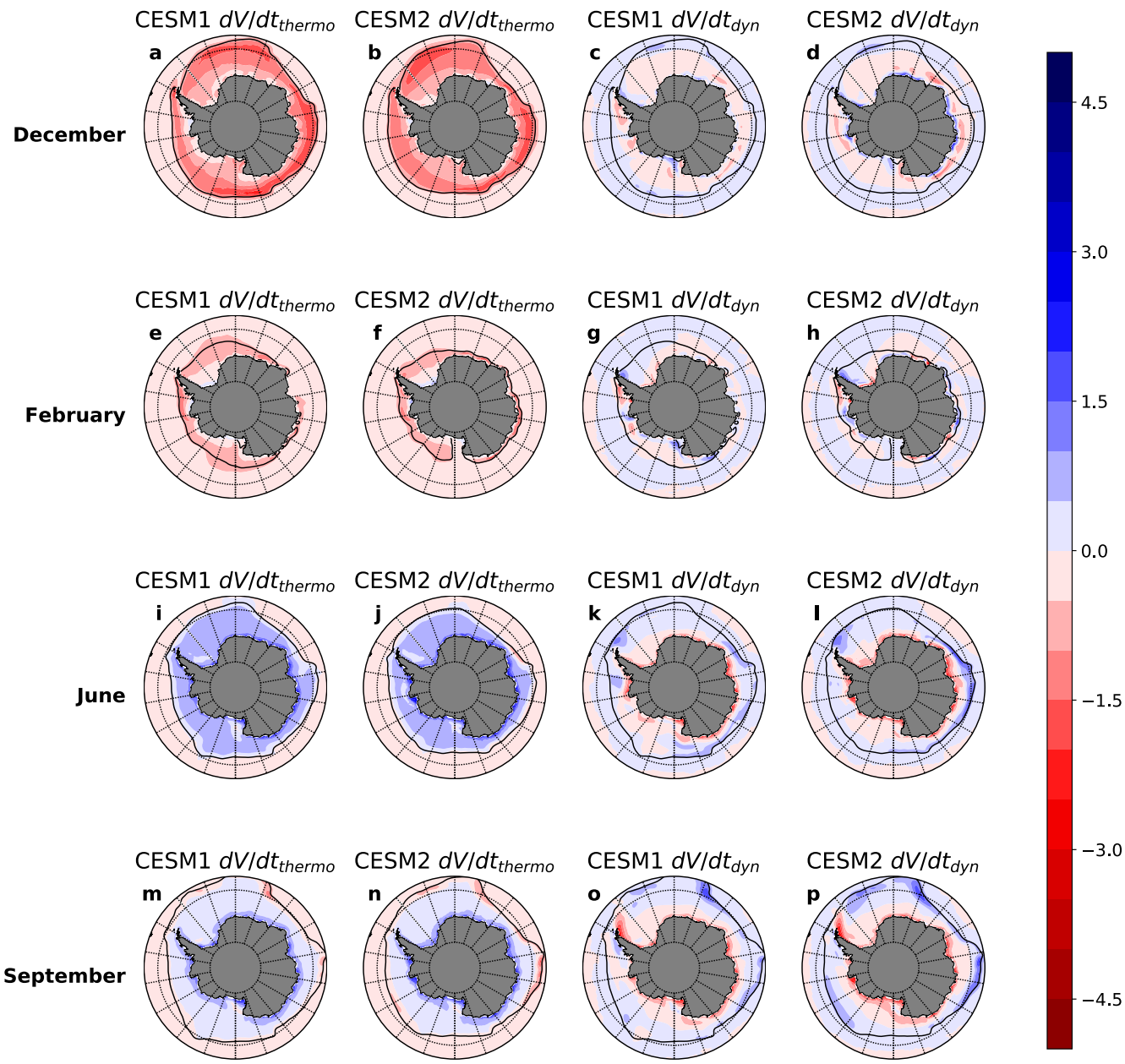

Figure 11. Thermodynamic and Dynamic Contributions to Antarctic Sea Ice Volume Change: Monthly mean (a, b, e, f, i, j, m, n) thermodynamic and (c, d, g, h, k, l, o, p) dynamic contributions to ice volume tendency dV/dt, in cm/day, in the (a, c, e, g, i, k, m, o) CESM1, and (b, d, f, h, j, l, n, p) CESM2. Shown for (a-d) December, (e-h) February, (i-l) June, and (m-p) September. In all panels, the black contour indicates sea ice extent (i.e. 0.15 ice fraction isoline).

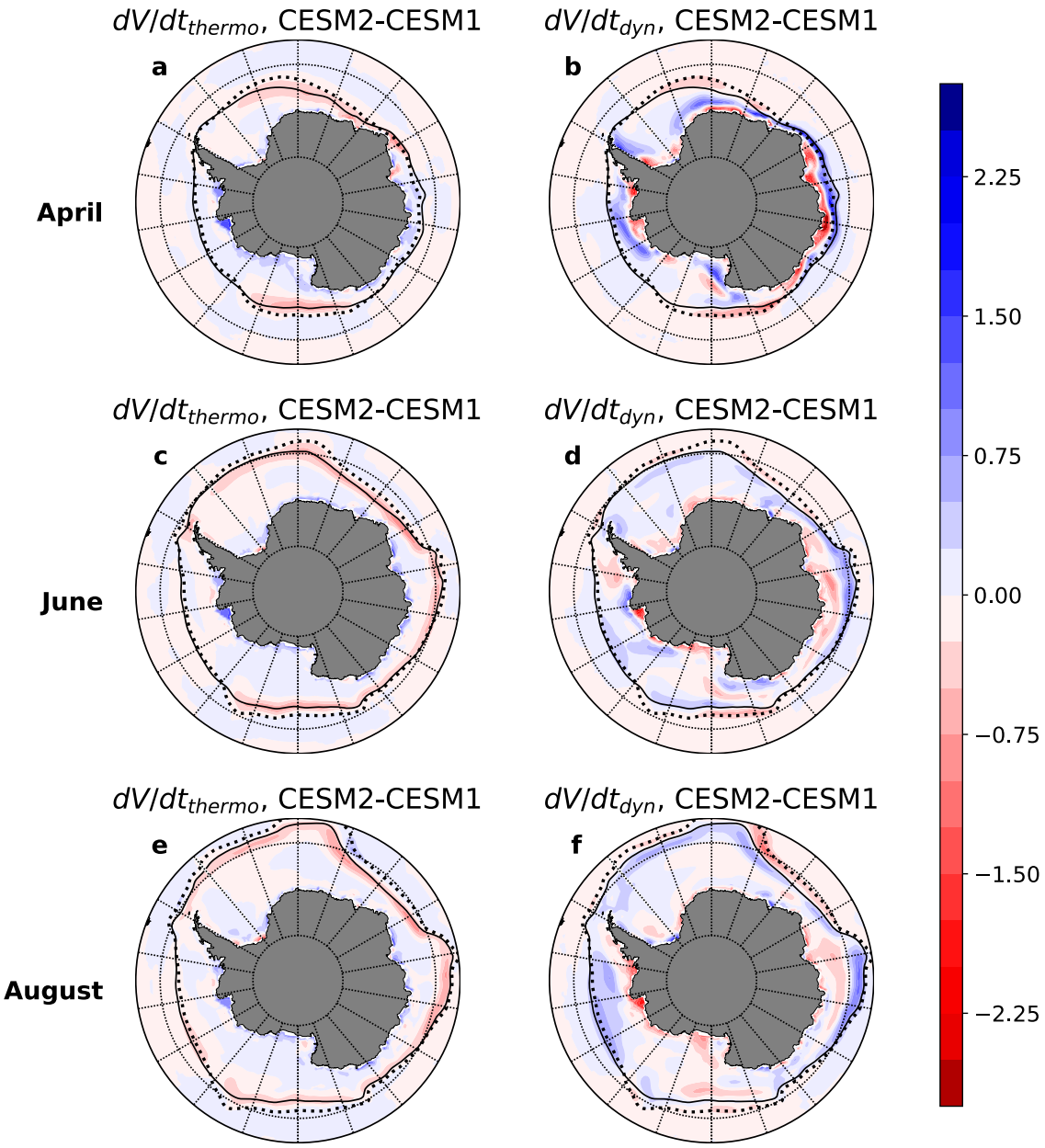

Figure 12. Differences in Thermodynamic and Dynamic Contributions to Antarctic Sea Ice Volume Change in the CESM2 versus the CESM1: Monthly mean difference in the (a, c, e) thermodynamic and (b, d, f) dynamic contributions to ice volume tendency dV/dt, in cm/day, between the CESM2 and the CESM1 (i.e. CESM2 minus CESM1). Shown for (a, b) April, (c, d) June, and (e,f) August. In all panels, the solid black contour indicates sea ice extent in the CESM2, and the dotted black contour indicates sea ice extent in the CESM1.

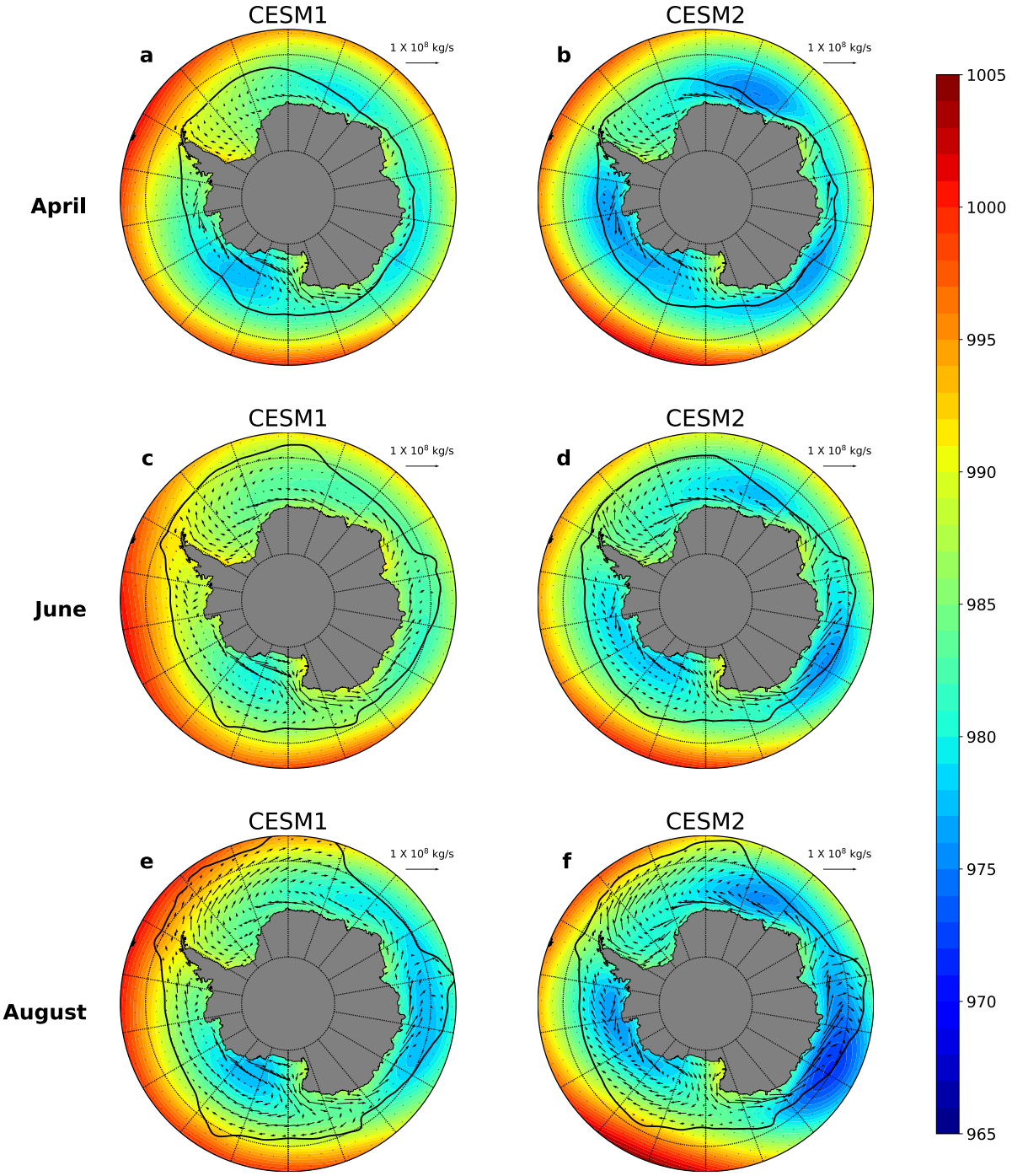

Figure 13. Antarctic Sea Ice Transport and Sea Level Pressure during the Growth Season: Monthly mean sea ice transport (vectors; in 10^8 kg/s) and sea level pressure (colors; in hPa) in the (a, c, e) CESM1 and (b, d, f) CESM2, in (a, b) April, (c, d) June, and (e, f) August.

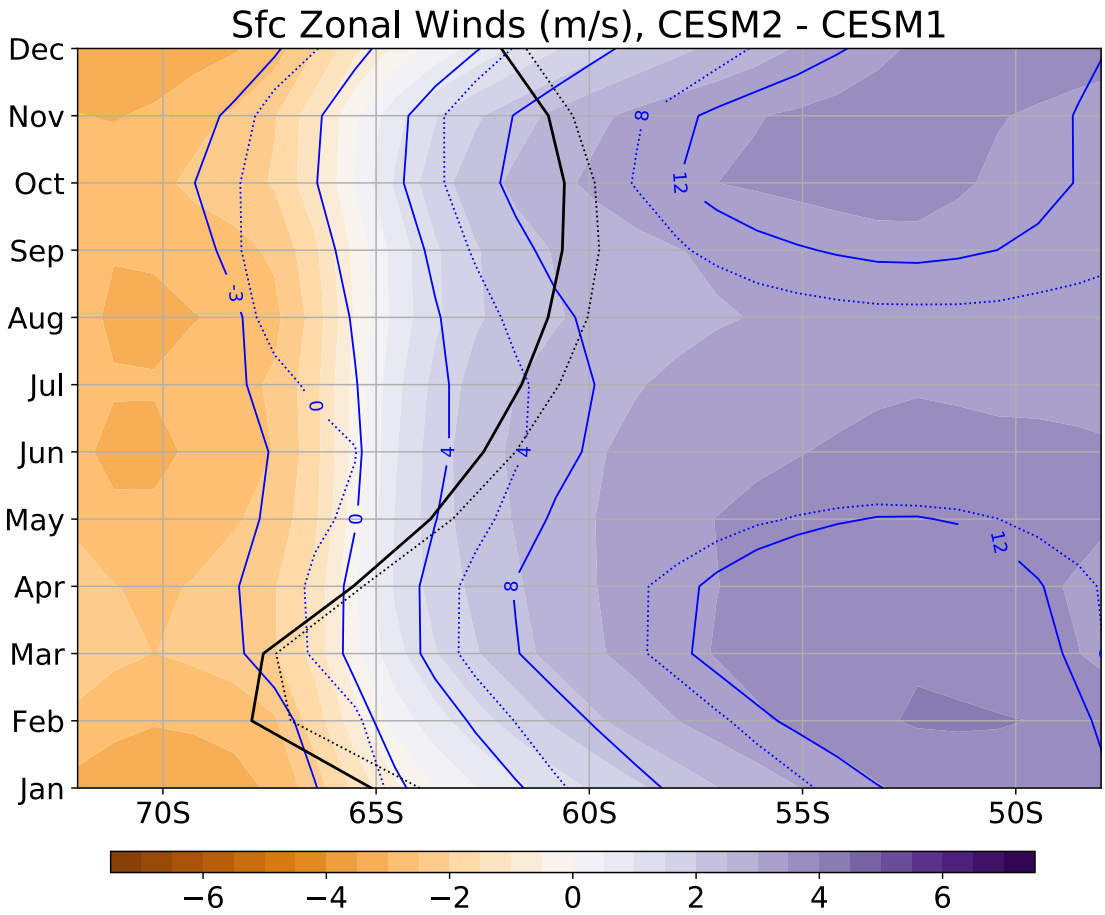

Figure 14. Zonal Winds at the Surface: Difference between the monthly zonal mean surface zonal winds in the CESM2 and CESM1 (in m/sec; colors). Blue solid and dotted contours (at -3, 0, 4, 8, 12 m/s) show the monthly zonal mean surface zonal winds in the CESM2 and CESM1, respectively. The monthly zonal mean ice extent (0.15 ice fraction isoline) for the CESM2 (CESM1) is indicated by the solid (dotted) black contour.

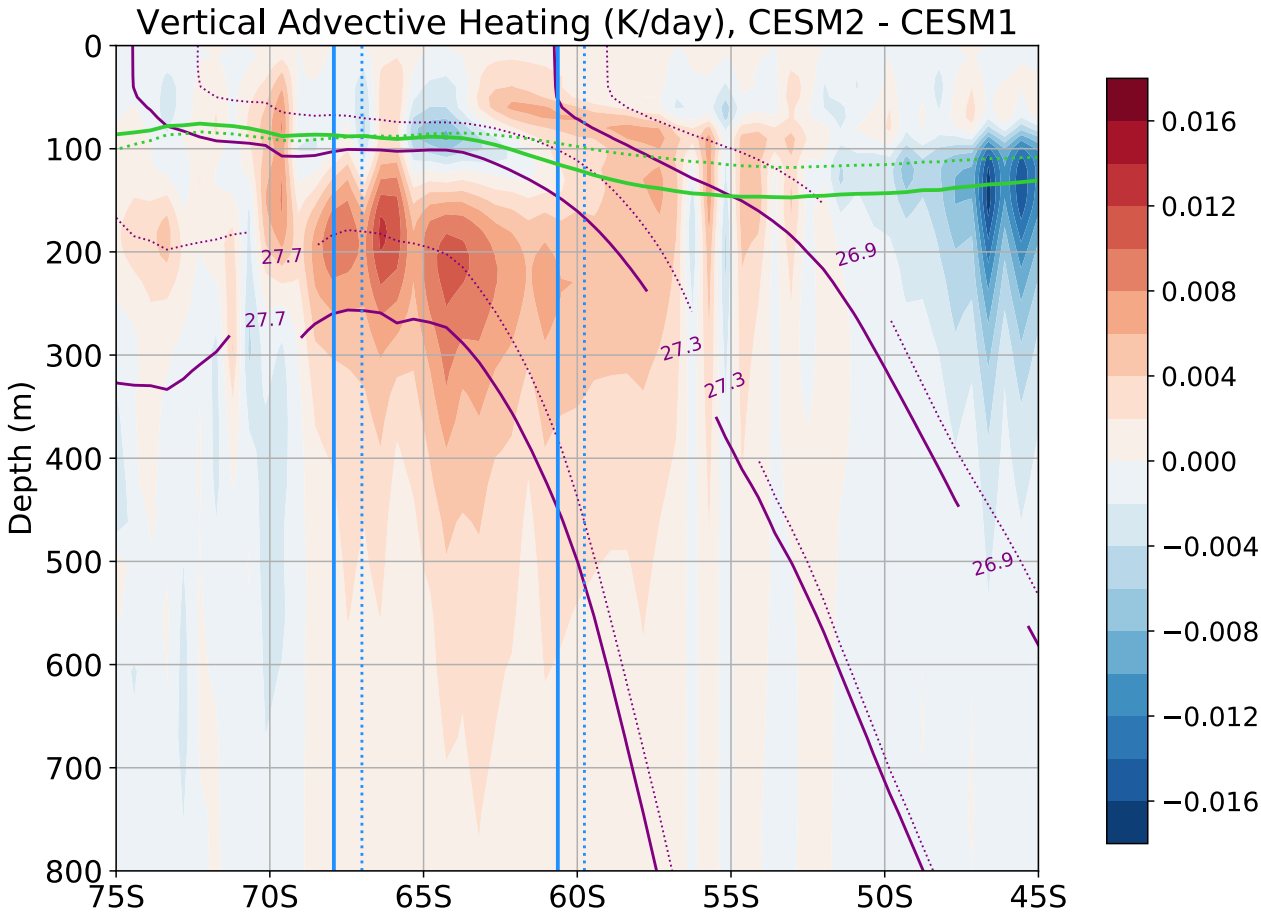

Figure 15. Heating by Upwelling during the Sea Ice Growth Season: Difference between ocean heating due to advection in the CESM2 and the CESM1 (in K/day; colors) over the growth season (March to August). Isopycnal surfaces (at $\sigma = 27.7, 27.3, 26.9$ kg/m^3) in the CESM2 and CESM1 are shown by the purple solid and dotted contours, respectively. The blue solid (dotted) lines show the range of the ice extent in the CESM2 (CESM1) from March to August, and the green solid (dotted) line indicates the zonal mean mixed layer depth in the CESM2 (CESM1) over the growth season.

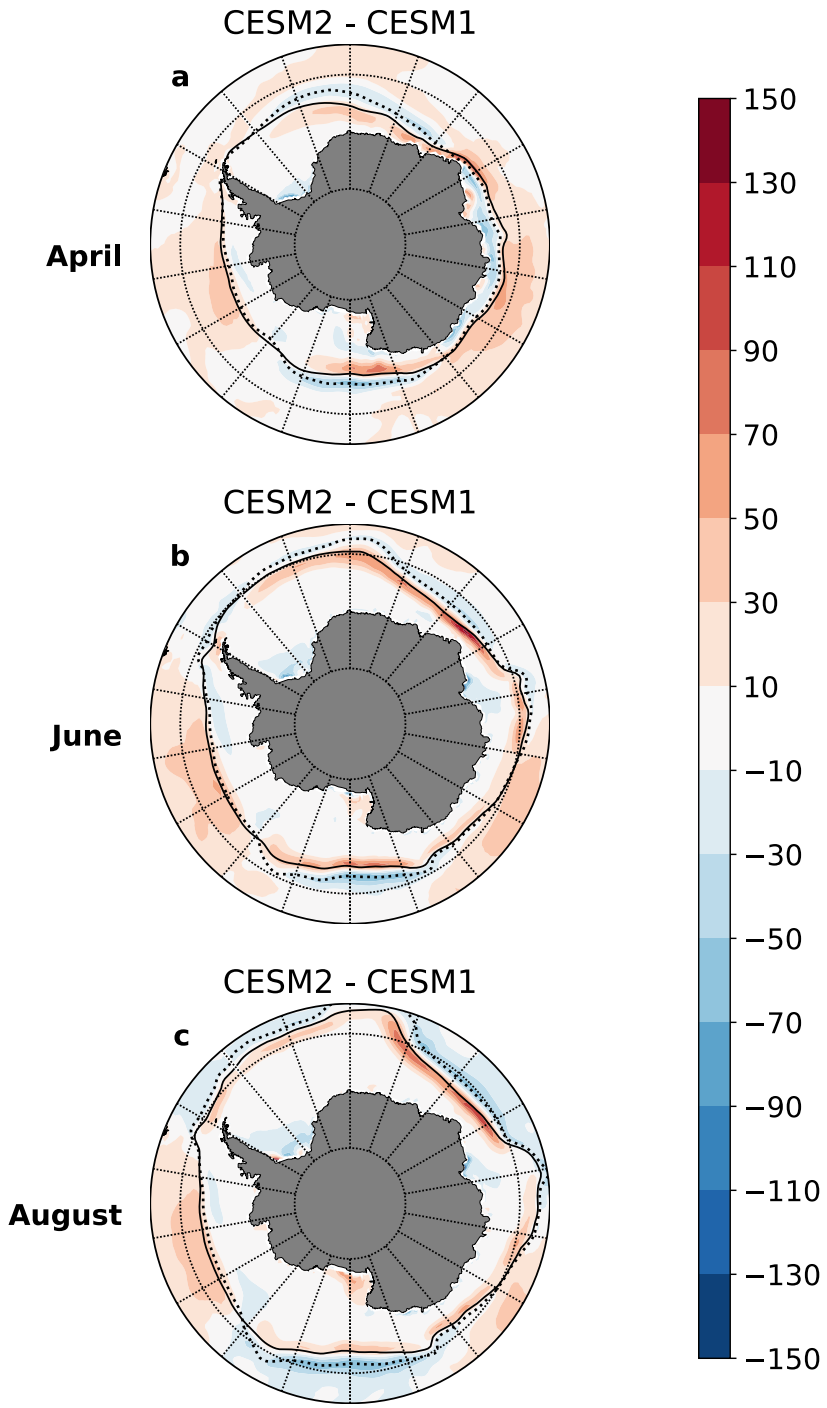

Figure 16. Ocean Heat Flux Convergence during the Sea Ice Growth Season: Difference between the monthly mean ocean heat flux convergence into the ocean mixed layer in the CESM2 and the CESM1 (in W/m^2; colors) in (a) April, (b) June, and (c) August. Solid and dashed contours in each panel show the sea ice extent in the CESM2 and CESM1, respectively.

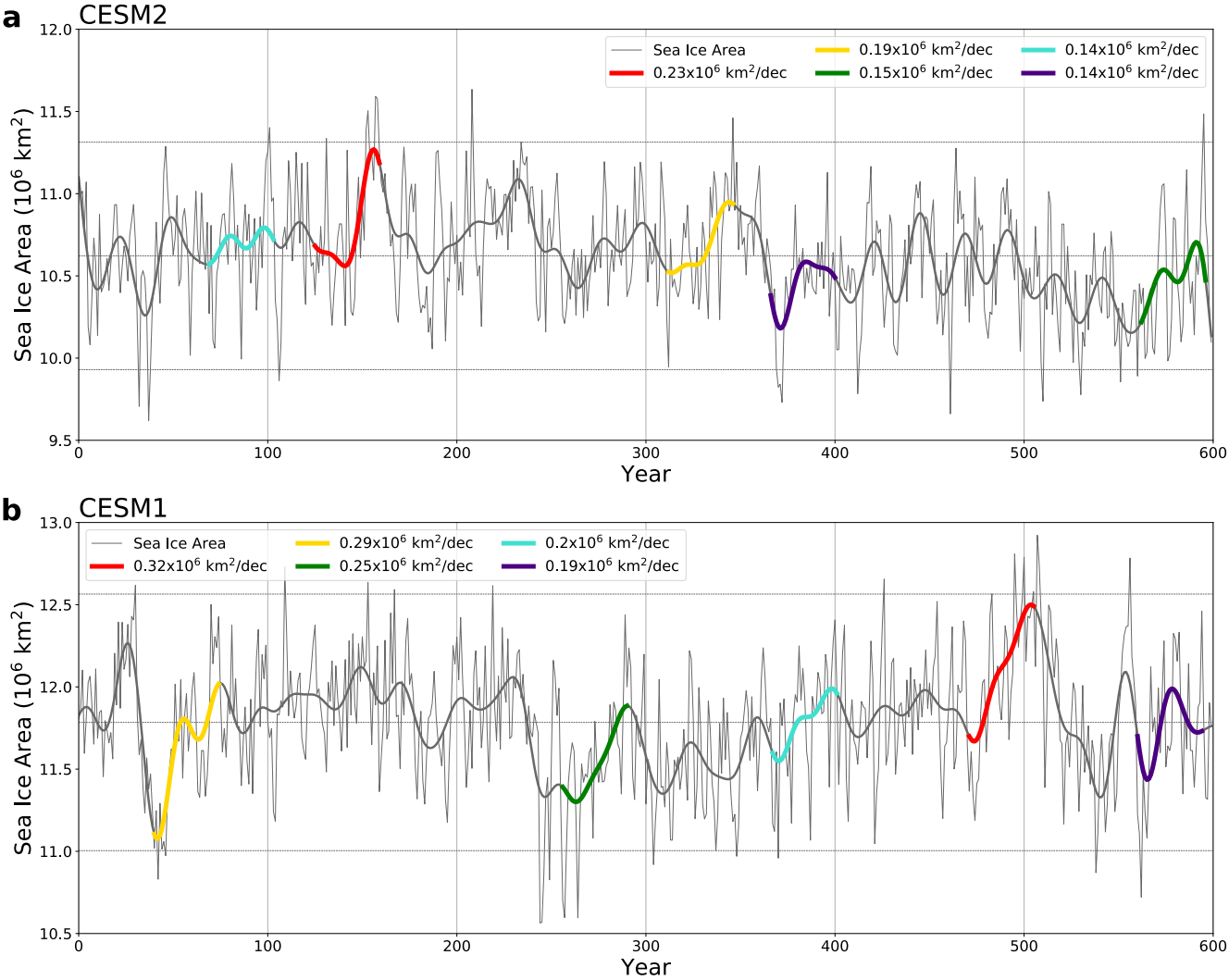

Figure 17. Variability in Annual Mean Antarctic Sea Ice Area: Annual mean Antarctic sea ice area (in 10^6 km^2) over 600 years, unfiltered (thin grey lines) and 10-yr low-pass filtered (thick grey and colored lines), in the (a) CESM2 and (b) CESM1. Colored line segments show the five 35-yr time periods with the greatest positive linear trends in sea ice area. Horizontal grey lines show the two standard deviation envelope of annual mean sea ice area.

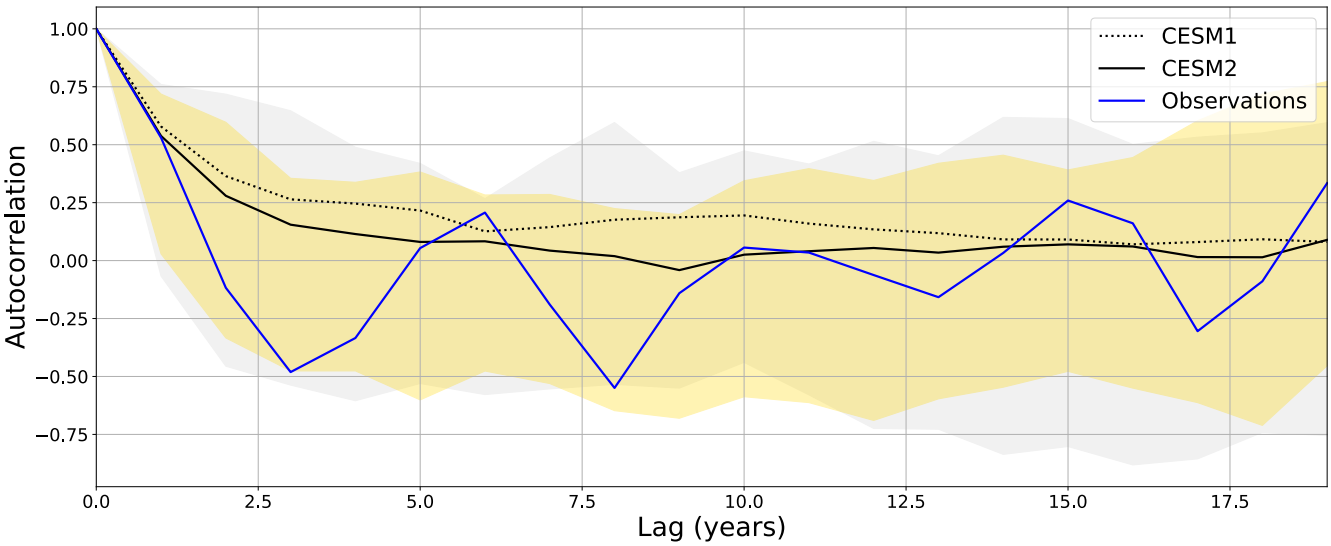

Figure 18. Autocorrelation of Annual Mean Antarctic Sea Ice Area: Lagged autocorrelation of annual mean Antarctic sea ice area in the CESM2 (solid black line), CESM1 (dotted black line), and the observational record (1979 to 2019; solid blue line). Shaded yellow (grey) area shows the range of the lagged autocorrelation, as calculated from all possible contiguous 40-yr segments of the CESM2 (CESM1) experiment.

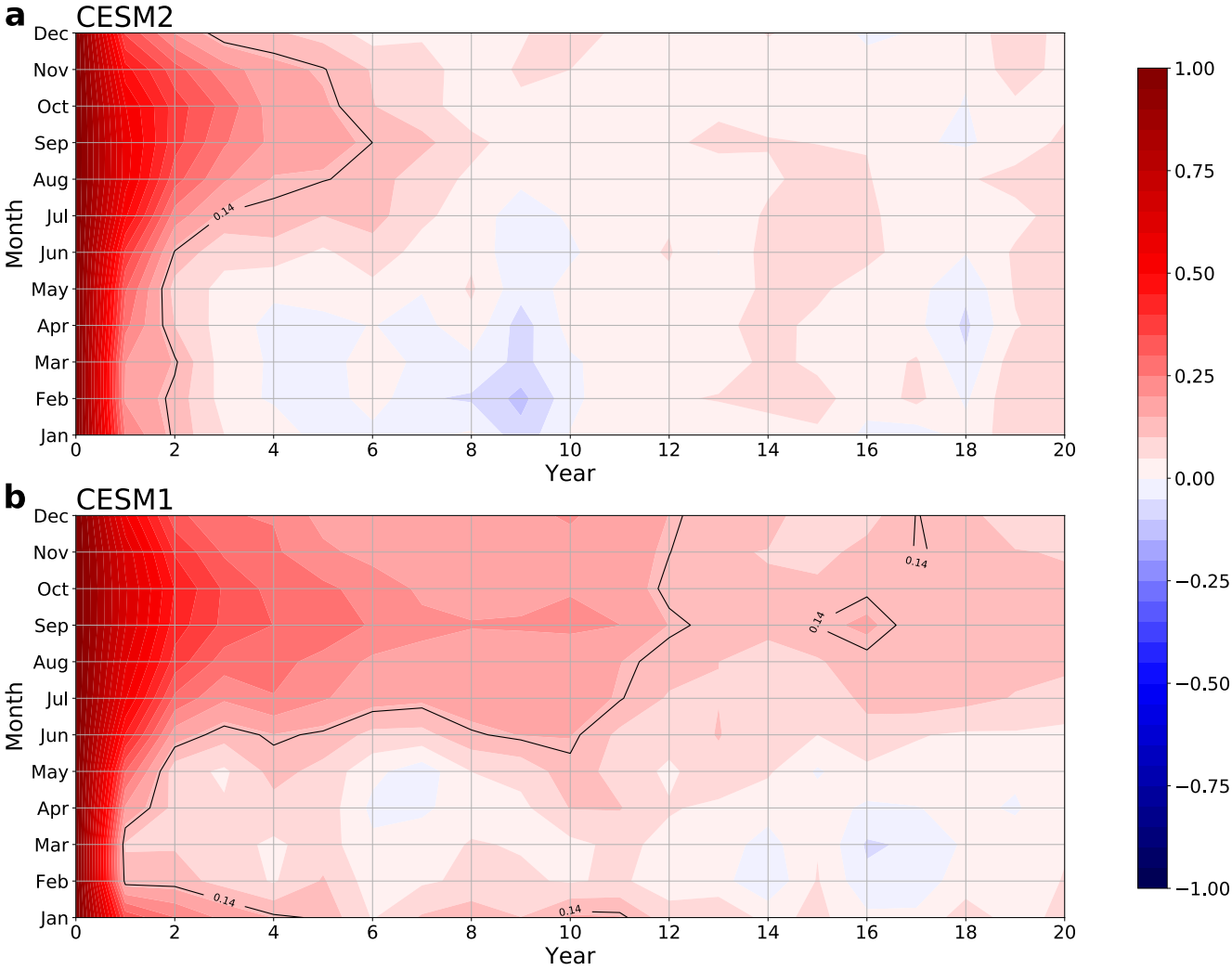

Figure 19. Autocorrelation of Monthly Mean Antarctic Sea Ice Area: Lagged autocorrelation of monthly mean Antarctic sea ice area in the (a) CESM2 and (b) CESM1. Black contours indicate the $r = 0.14$ correlation isoline; correlations greater than this value are statistically significant at $p < 0.05$.

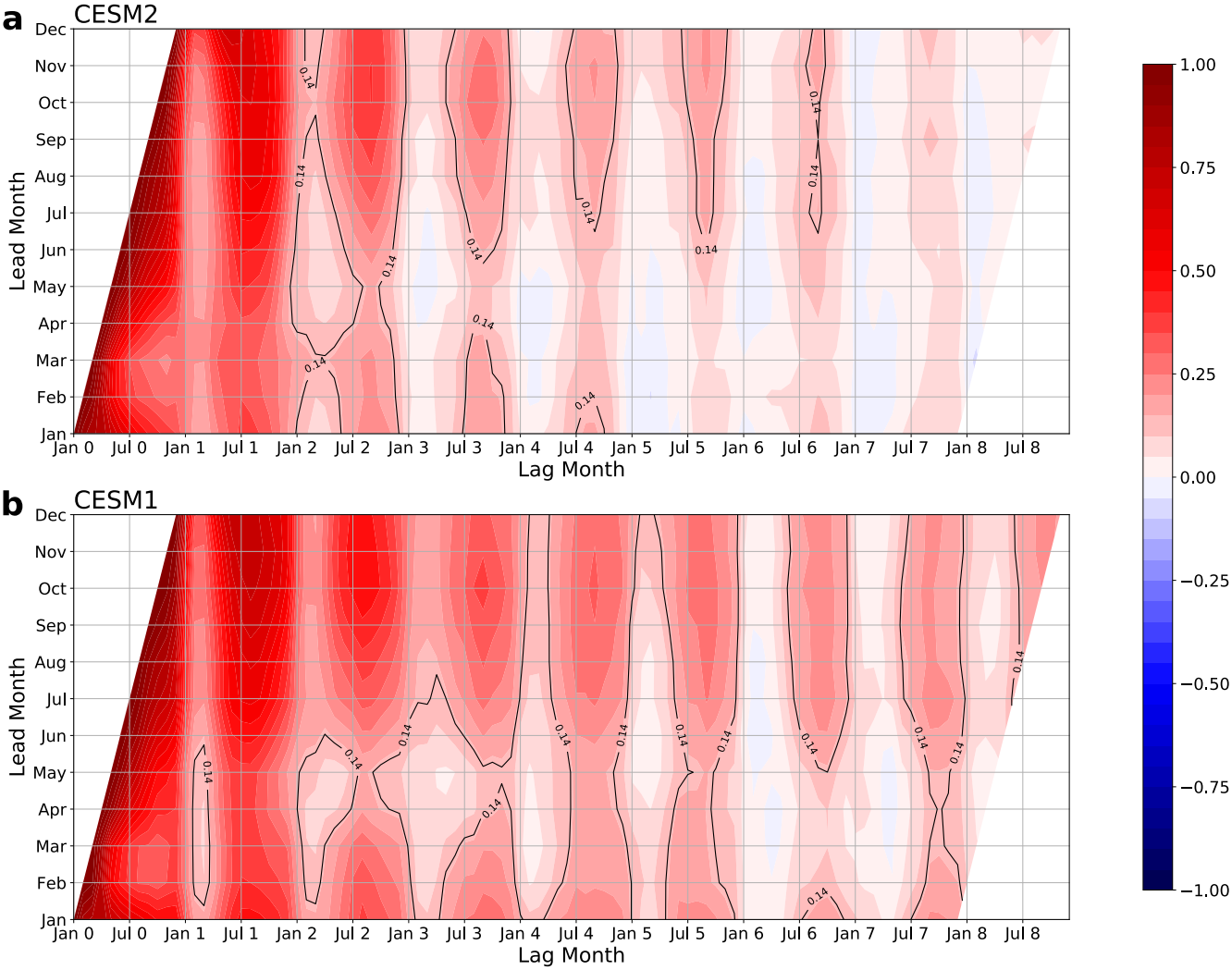

Figure 20. Predictability of Monthly Antarctic Sea Ice Area: Lead-lag correlations between monthly sea ice area in the (a) CESM2 and (b) CESM1, with the lead (i.e. predictor) month on the vertical axis and the lag (i.e. predictand) month on the horizontal axis. For the lag month, '0' refers to the current year, '1' refers to first following year, '2' refers to the second following year, and so forth. Black contours highlight the $r = 0.14$ correlation isoline; correlations greater than this value are statistically significant at $p < 0.05$.

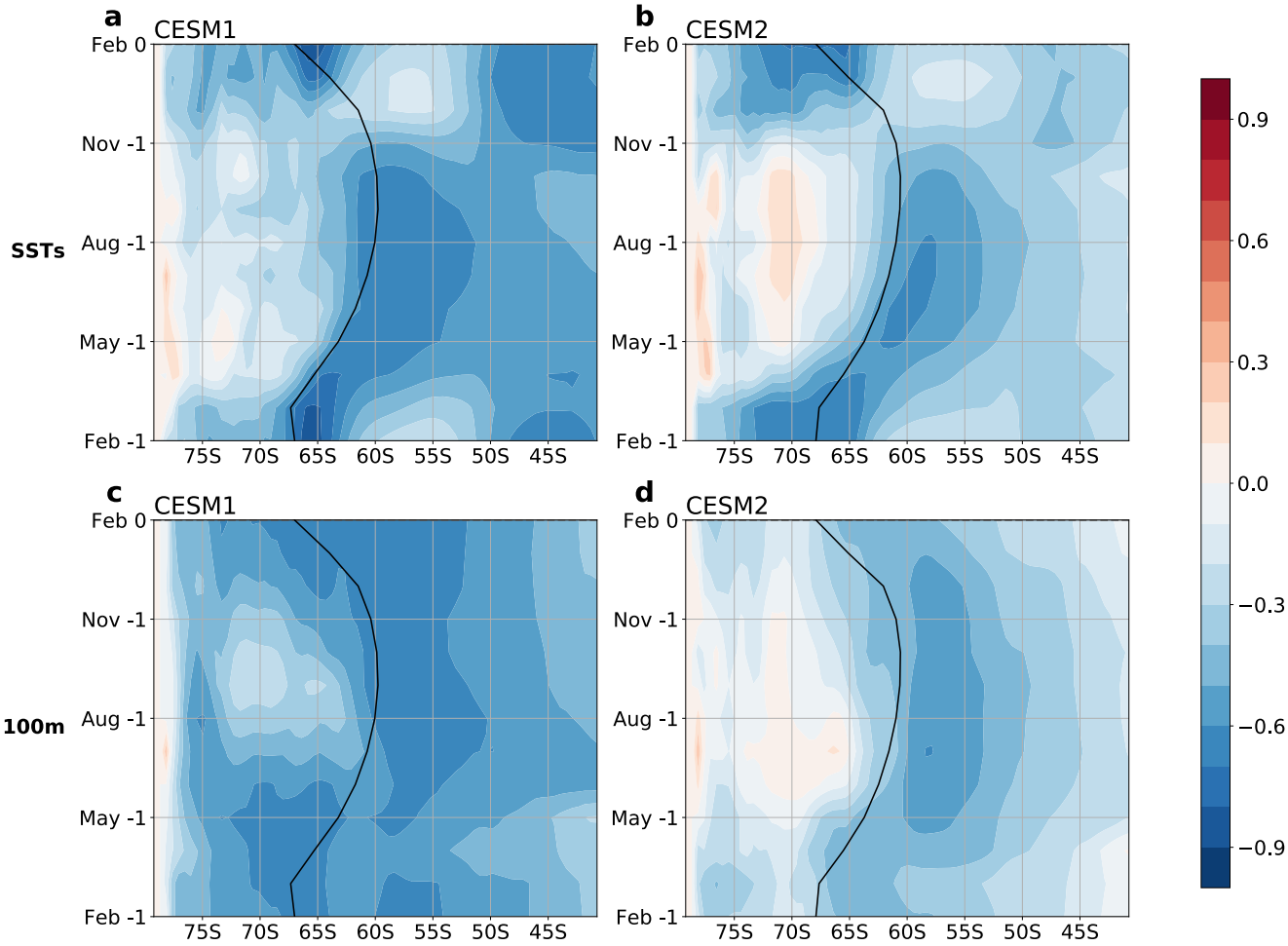

Figure 21. Relationships Between February Sea Ice Area and Ocean Temperatures over Previous Twelve Months: Correlations between February sea ice area and (a, b) zonal mean SSTs and (c, d) zonal mean 100m-depth ocean temperatures in (a, c) CESM1 and (b, d) CESM2. Ocean temperatures precede sea ice area, except for concurrent 'Feb 0' temperatures; '-1' indicates correlations between sea ice area and ocean temperatures over individual months from the previous year. The black contour shows the zonal mean ice edge.

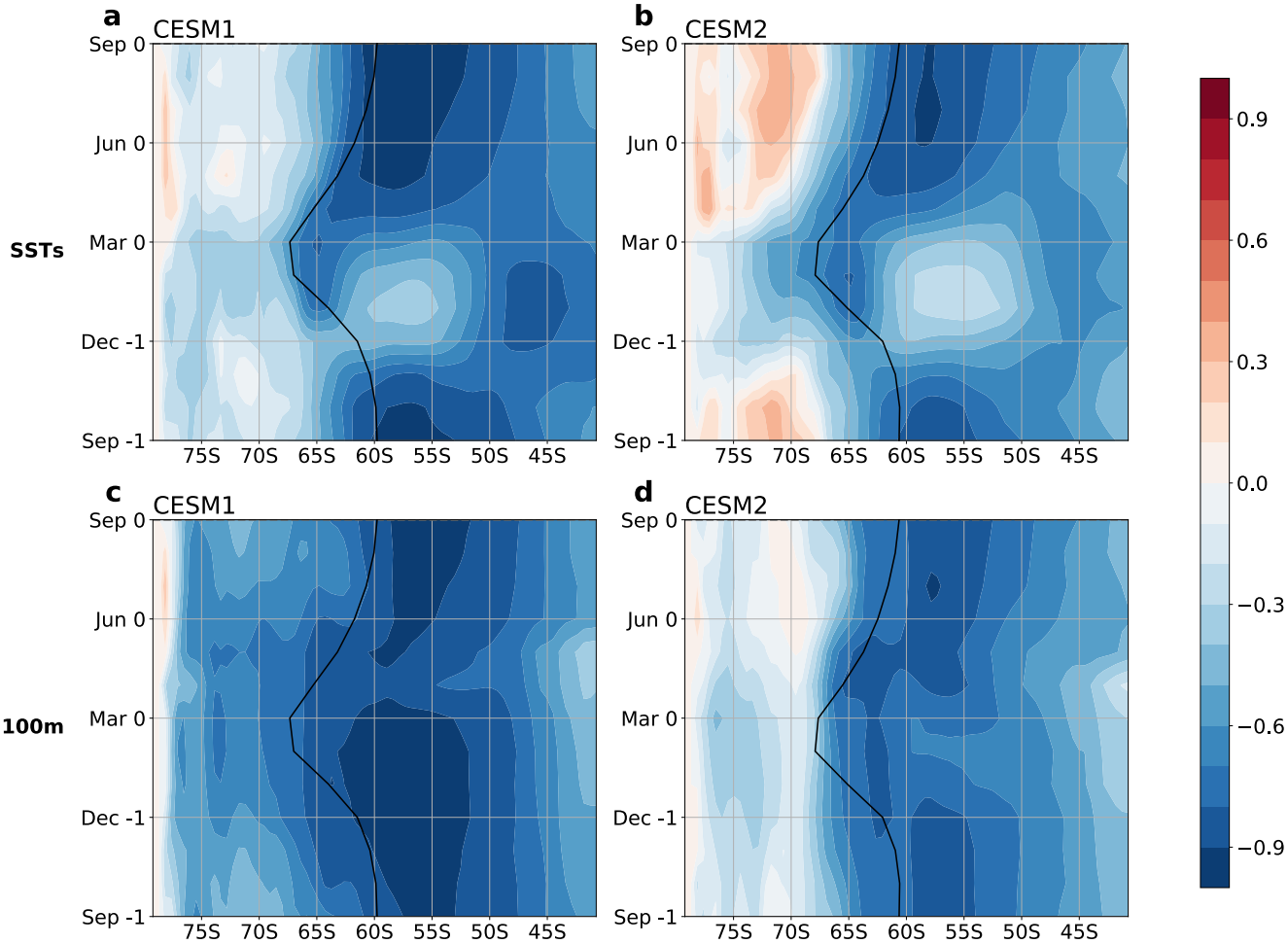

Figure 22. Relationships Between September Sea Ice Area and Ocean Temperatures over Previous Twelve Months: Lead-lag correlations between September sea ice area and (a, b) zonal mean SSTs and (c, d) zonal mean 100m-depth ocean temperatures in (a, c) CESM1 and (b, d) CESM2. Ocean temperatures precede sea ice area, except for concurrent 'Sep 0' temperatures; '-1' indicates correlations between sea ice area and ocean temperatures over individual months from the previous year. The black contour shows the zonal mean ice edge.

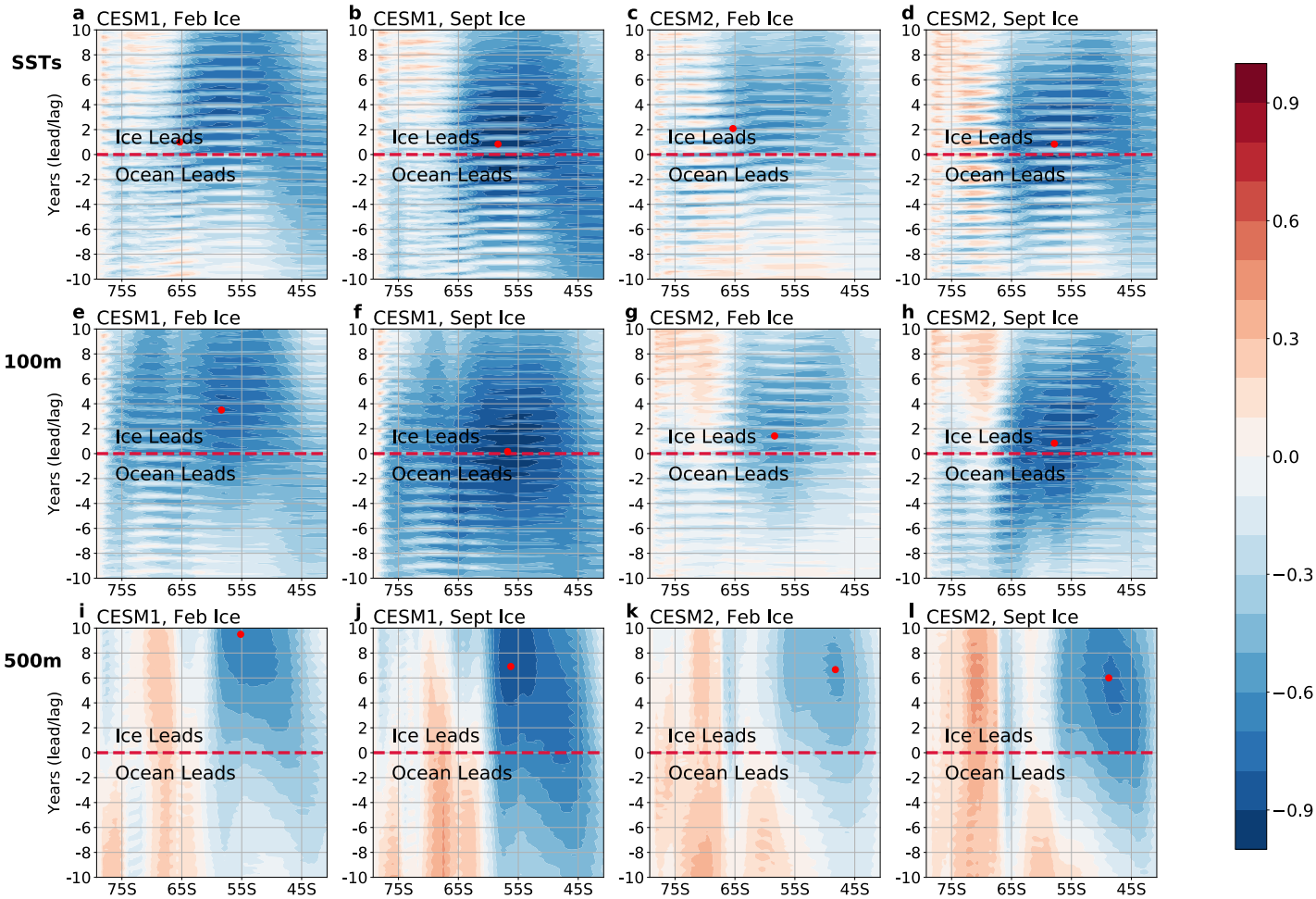

Figure 23. Lead-Lag Relationships Between Sea Ice Area and Ocean Temperatures over Decadal Time Scales: Lead-lag correlations between (b, d, f, h, j, l) September sea ice area or (a, c, e, g, i, k) February sea ice area and monthly-mean, zonal-mean (a-d) SSTs, (e-h) ocean temperatures at 100m depth, or (i-l) ocean temperatures at 500m depth. Shown for the (a, b, e, f, i, j) CESM1 and (c, d, g, h, k, l) CESM2. The dashed red line indicates the correlation between sea ice area and ocean temperatures at zero lead-lag, and the red dot indicates the lead-lag and latitude where the correlation is most negative.

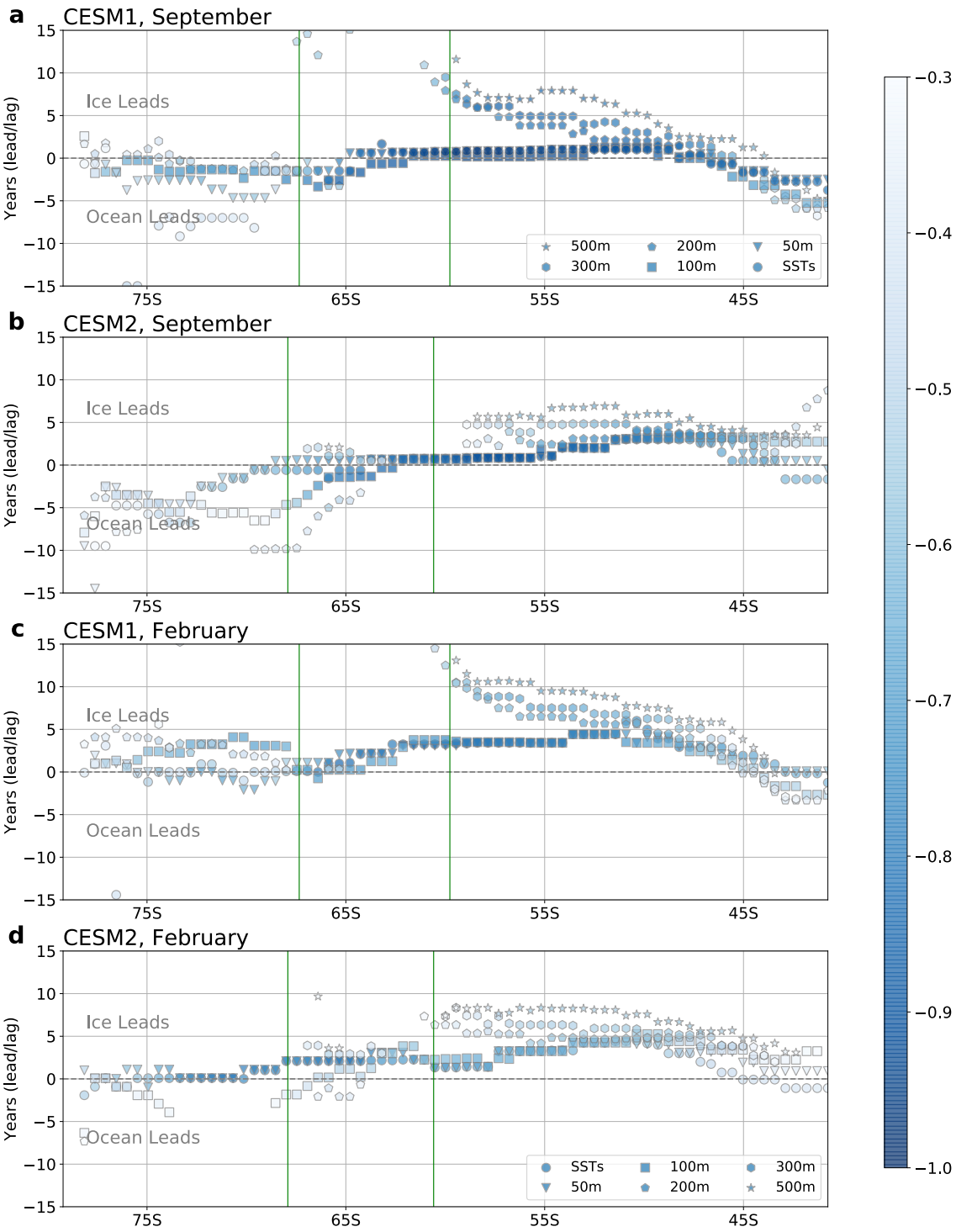

Figure 24. Strongest Lead-Lag Relationships (by latitude) Between Sea Ice Area and Ocean Temperatures over Decadal Time Scales: Lead-lag of maximum negative correlations (colors of markers) at each latitude between monthly-mean zonal-mean ocean temperatures (markers; SSTs, and ocean temperatures at 50m, 100m, 200m, 300m, and 500m depth) and (a, b) September sea ice area and (c, d) February sea ice area, for the (a, c) CESM1 and (b, d) CESM2. Only correlations that exceed $r = -0.3$ are shown.